Further improvement of wet process treatments in GEOS-Chem v12.6.0: Impact on global distributions of aerosols and aerosol precursors

Gan Luo[1], Fangqun Yu[1], Jonathan M. Moch[2]

[1]Atmospheric Sciences Research Center, University at Albany, Albany, NY, USA

[2]Department of Earth and Planetary Sciences, Harvard University, Cambridge, MA, USA

Abstract

Wet processes, including aqueous phase chemistry, wet scavenging, and wet surface uptake during dry deposition, are important for global modeling of aerosols and aerosol precursors. In this study, we improve the treatments of these wet processes in the GEOS-Chem v12.6.0, including pH calculations for cloud, rain, and wet surfaces, the fraction of cloud available for aqueous phase chemistry, rainout efficiencies for various types of clouds, empirical washout by rain and snow, and wet surface uptake during dry deposition. We compare simulated surface mass concentrations of aerosols and aerosol precursors with surface monitoring networks over the United States, Europe, Asia, and Arctic regions, and show that model results with updated wet processes agree better with measurements for most species. With the implementation of these updates, normalized mean biases (NMB) of surface nitric acid, nitrate, and ammonium are reduced from 78%, 126%, and 45% to 0.9%, 15%, and 4.1% over the US sites, from 107%, 127%, and 90% to -0.7%, 4.2%, and 16% over Europe sites, and from 121%, 269%, and 167% to -21%, 37%, and 86% over Asia remote region sites. Comparison with surface measured SO_2, sulfate and black carbon at four Arctic sites indicated that these species simulated with the updated wet processes match well with observations except for a large underestimate of black carbon at one of the sites. We also compare our model simulation with aircraft measurement of nitric acid and aerosols during the ATom-1 and ATom-2 periods and found a significant improvement of modeling skill of nitric acid, sulfate, and ammonium in the Northern Hemisphere during winter time. The NMBs of these species are reduced from 163%, 78%, and 217% to -13%, -1%, and 10%, respectively. The investigation of impacts of updated wet process treatments on surface mass concentrations indicated that the updated wet processes have strong impacts on the global means of nitric acid, sulfate, nitrate, and ammonium and

relative small impacts on the global means of sulfur dioxide, dust, sea salt, black carbon, and organic carbon.

1. Introduction

Aqueous phase chemistry, wet scavenging, and wet surface uptake during dry deposition are the three major atmospheric wet processes for aerosols and aerosol precursors. Aqueous phase chemistry plays a role as reaction chamber which efficiently converts aerosol precursors to aerosols (Ervens et al.,2011; Walcek and Taylor,1986). Wet scavenging, a process by which chemicals accumulate in droplets and then are removed by precipitation, is the predominant removal pathway of aerosols and aerosol precursors (Textor et al., 2006). Dry deposition, where chemicals settle out of the atmosphere in the absence of precipitation, is greatly enhanced due to the absorption of water soluble gases at wet surfaces associated with dew, fog, and rain (Garland and Branson, 1977; Wesely, 1989). These wet processes significantly impact global mass load and redistribute aerosols and aerosol precursors. Aerosol mass load and its global distributions are important for studies of aerosol optical properties (Kinne et al., 2006), aerosol direct radiative forcing (Myhre et al., 2013; Penner et al., 1994), and the health effects of particulate matter (Shiraiwa et al., 2017; Hopke et al., 2006). A better representation of wet processes in global modeling of aerosols and aerosol precursors can therefore enhance our ability to accurately simulate these different aerosol impacts.

GEOS-Chem is a widely used community model which is continuously being improved (Holmes et al., 2019; Keller et al., 2014; Martin et al., 2003; Bey et al., 2001). Luo et al. (2019), L2019 hereafter, updated the GEOS-Chem wet scavenging scheme by using the Modern-Era Retrospective analysis for Research and Applications, Version 2 (MERRA-2) spatially and temporally varying cloud and rain water to replace the assumption of fixed in-cloud condensation water (ICCW) in the GEOS-Chem rainout parameterization and by using new empirical rates for nitric acid and water soluble aerosols in washout. These changes together reduced the normalized mean biases (NMB) of simulated nitric acid, nitrate, and ammonium mass concentrations at the United States' surface monitoring networks from 145%, 168%, and 81% to 24%, 25%, and 13%, respectively. However, the impacts of the updated wet scavenging scheme on simulations over other regions (Europe, Asia, and remote areas) and free troposphere were not investigated. Moreover, L2019 only investigated the changes of nitric acid, nitrate, and

ammonium. The impact of the updated wet scavenging scheme on other aerosols such as sulfate, sea salt, dust, and carbonaceous aerosols was not investigated in that work. Due to the large impact of updated wet scavenging on model simulations, a comprehensive validation of simulated aerosols and aerosol precursors with ground based monitoring networks for surface mass concentrations and aircraft measurements for vertical profiles is needed.

In this study, we further update the treatments of wet processes (aqueous chemistry, wet scavenging, and wet surface uptake during dry deposition) in GEOS-Chem and evaluate comprehensively simulated major inorganic aerosol precursors (sulfur dioxide, nitric acid, and ammonia) and aerosols (sulfate, nitrate, ammonium, black carbon, and organic carbon) by comparison with a large set of in-situ observations. The updates to the wet processes are detailed in Section 2. Comparisons of simulations with measurements from surface monitoring networks including the United States Environmental Protection Agency (USEPA), the Interagency Monitoring of Protected Visual Environments (IMPROVE), the Chemical Speciation Network (CSN), the Clean Air Status and Trends Network (CASTNET), the Ammonia Monitoring Network (AMoN), the National Trends Network (NTN), the European Monitoring and Evaluation Programme (EMEP), and the Acid Deposition Monitoring Network in East Asia (EANET) are given in section 3.1. Validations of aerosols and aerosol precursors for the Arctic and the Atmospheric Tomography (ATom) mission are presented in sections 3.2 and 3.3. The impact of the updated wet processes on global surface concentrations or aerosols and aerosol precursors are discussed in section 3.4. A summary of our results is given in section 4.

2 Updates of wet process treatments in GEOS-Chem associated with aerosol precursor and aerosol modeling

In the publicly released GEOS-Chem version 12.6.0, GC12 thereafter, in-cloud aqueous phase chemistry was developed by Chin et al. (2000) for SO_2. The wet scavenging scheme, including rainout due to formation of precipitation from clouds and washout due to falling precipitation from upper layers, was developed by Jacob et al. (2000) and Liu et al. (2001) for aerosols and by Amos et al. (2012) for gases. Scavenging of aerosol by snow and cold–mixed precipitation was updated by Wang et al. (2011, 2014). Wet surface uptake during dry deposition is represented with constant values of effective Henry's law coefficient for surface resistance

1 calculations   (http://wiki.seas.harvard.edu/geos-chem/index.php/Physical_properties_of_GEOS-

2 Chem_species#Definition_of_Henry.27s_law_constants).

3   L2019 showed that the assumption of in-cloud condensation water with a fixed value (1

4 $g \cdot m^{-3}$) in the rainout parameterization in GC12 is one of the major reasons causing an

5 overestimate in nitrate and ammonium mass concentrations compared to surface monitoring

6 networks over the US. After replacing the fixed value of in-cloud condensation water with

7 MERRA-2 cloud and rain water, we get an updated equation for rainout loss fraction (Luo et al.,

8 2019):

9 $$F = \frac{P_r}{k \cdot \text{ICCW}}\left(1 - e^{-k \cdot \Delta t}\right) = \frac{f_c \cdot P_r}{k\left(\text{LCW} + \text{ICW} + P_r \cdot \Delta t\right)}\left(1 - e^{-k \cdot \Delta t}\right), (1)$$

10 where F is the fraction of a water-soluble tracer in the grid-box scavenged by rainout, Δt (s) is

11 the model integration time step. k is the first-order rainout loss rate which represents the

12 conversion of cloud water to precipitation water. ICCW ($g \cdot m^{-3}$) is in-cloud condensation water.

13 P_r ($g \cdot m^{-3} \cdot s^{-1}$) is the rate of new precipitation formation. f_c, LCW ($g \cdot m^{-3}$), and ICW ($g \cdot m^{-3}$) are the

14 grid-box mean cloud fraction, , liquid phase cloud water content, and ice phase cloud water

15 content, respectively.

16   L2019 also showed that the difference between observations and simulations can be

17 further reduced, through (1) the update of empirical washout coefficients by rain for water-

18 soluble aerosol with the value which was calculated by the parameterization of Laakso et al.

19 (2003) for a 500 nm particle diameter, and (2) the new estimated washout coefficients for nitric

20 acid by referring to field measurements for particles with a 10 nm diameter (Laakso et al., 2003)

21 and the theoretical dependence of scavenging coefficients on particle sizes for particles < 10 nm

22 (Henzing et al., 2006). L2019 only focused on warm cloud wet scavenging, and did not

23 systematically consider the impact of wet process treatments on the simulated aerosols and

24 aerosol precursors. Here we show that a number of treatments in GC12 and L2019 can be further

25 updated (as detailed below) to improve the performance of GEOS-Chem in simulating spatial

26 and temporal variations of major aerosols and aerosol precursors on a global scale.

27

28 **2.1 pH for cloud, rain, and wet surface**

1   Water pH is important for dissolution and subsequent aqueous phase reactions of water-

2   soluble gases (Turnock et al., 2019; Ervens, 2015; Pandis and Seinfeld, 1989). Based on Henry's

3   law, dissolution of water-soluble gases can be calculated as:

4    $$f_w = 1 - \frac{1}{1 + H^* \cdot R \cdot T \cdot LW}, \quad (2)$$

5   where f_w is the dissolution fraction for water-soluble gases, H^* (mol·L^{-1}·atm^{-1}) is effective

6   Henry's law constant, R (0.08205 L·atm·K^{-1}·mol^{-1}) is the gas constant, T (K) is the temperature,

7   and LW (m^3·m^{-3}) is the liquid water content.

8   H^* represents the impact of temperature, water acidity, and aqueous phase equilibrium on

9   solubility of water-soluble species (Seinfeld and Pandis, 2016). For SO$_2$, H$_2$O$_2$, and NH$_3$, which

10   are important for aerosol precursor and aerosol simulation, H^* can be calculated as (Seinfeld and

11   Pandis, 2016):

12   $$\left.\begin{array}{l} H^*_{SO2} = H_{SO2}\left(1 + \dfrac{K_1}{[H^+]} + \dfrac{K_1 \cdot K_2}{[H^+]^2}\right), \\[2mm] H_{SO2} = 1.22 e^{10.55\left(\frac{298.15}{T}-1\right)}, \\[2mm] K_1 = 1.3\times10^{-2} e^{6.75\left(\frac{298.15}{T}-1\right)}, \\[2mm] K_2 = 6.31\times10^{-8} e^{5.05\left(\frac{298.15}{T}-1\right)} \end{array}\right\} \quad (3)$$

13   $$\left.\begin{array}{l} H^*_{H2O2} = H_{HO2}\left(1 + \dfrac{K_3}{[H^+]}\right), \\[2mm] H_{H2O2} = 8.3\times10^4 e^{24.82\left(\frac{298.15}{T}-1\right)}, \\[2mm] K_3 = 2.2\times10^{-12} e^{12.52\left(\frac{298.15}{T}-1\right)} \end{array}\right\} \quad (4)$$

14   $$\left.\begin{array}{l} H^*_{NH3} = H_{NH3}\left(1 + \dfrac{K_5[H^+]}{K_4}\right), \\[2mm] H_{NH3} = 59.8 e^{14.1\left(\frac{298.15}{T}-1\right)}, \\[2mm] K_4 = 1.\times10^{-14} e^{-22.5\left(\frac{298.15}{T}-1\right)}, \\[2mm] K_5 = 1.7\times10^{-5} e^{-14.5\left(\frac{298.15}{T}-1\right)} \end{array}\right\} \quad (5)$$

1 where H_{SO2}, H_{H2O2}, and H_{NH3} are the Henry's law constants (M atm^{-1}) for SO_2, H_2O_2, and NH_3,

2 respectively. K_1 (M), K_2 (M), K_3 (M), K_4 (M^2), and K_5 (M) are rate coefficients for SO_2 reaction,

3 HSO_3^- reaction, H_2O_2 reaction, H_2O reaction, and NH_3 reaction, respectively. The values of the

4 Henry's law constants and rate coefficients are the same as those used in GEOS-Chem aqueous

5 phase chemistry. [H$^+$] (M) is the hydrogen ion concentration in cloud/rain droplets and at wet

6 surfaces, which is related to pH as:

7 $[H^+]=10^{-pH}$, (6)

8   GC12 calculates cloud water pH iteratively by using the concentrations of sulfate, total

9 ammonium (ammonium + ammonia), total nitrate (nitrate + nitric acid), SO_2, and CO_2 based on

10 their effective Henry's law coefficients and cloud liquid water content in corresponding grid box

11 (Alexander et al., 2012). This iterative calculation is updated to use Newton's method in order to

12 arrive at a consistent result (Moch et al., 2020). To implement Newton's method the equilibrium

13 expressions for the concentrations of each soluble semi-volatile ion (SSVI) in terms of H+ and

14 the derivatives for these equilibrium expressions are each solved explicitly so that the Newton's

15 method equation is in the form of:

16 $$H_{n+1}^+ = H_n^+ + \frac{\left[SSVI\left(H_n^+\right)\right]+[SNVI]}{\dfrac{d}{dH^+}\left[SSVI\left(H_n^+\right)\right]} , (7)$$

17 where SNVI is the concentrations of soluble nonvolatile ions. For equation (7) the concentrations

18 of each ion are multiplied by the ion charge (e.g. the terms for SO_3^{2-} concentrations are

19 multiplied by -2).

20   In tests with this new calculation the solution always converged to an answer in less than

21 20 iterations, but if a maximum of 50 iterations is reached we set it so that the last two solutions

22 are averaged together. We here considered the solution to converge if the difference between H_n^+

23 and H_{n+1}^+ was less than 0.01. By default the initial guess for H$^+$ is set to 4.5, but we tested initial

24 guesses ranging from a pH of 2 to 13 and found no change in the values at which the answer

25 converged.

26   To represent the removal of aerosols due to rainout, GC12 assumes 30% of sulfate,

27 nitrate, and ammonium are removed away from cloud water before cloud water pH calculation.

28 To take into account the variations in the amount of these species rained out, we use the real-time

1   rainout fractions for corresponding species which are calculated during the treatment of wet

2   scavenging to replace this constant value (i.e., 30%). Additionally, in GC12, sulfate is assumed

3   to be the only SNVI in cloud water, while ammonium and nitrate are treated as volatile species

4   similar to ammonia and nitric acid:

5    $[\text{SNVI}] = 2\left[\text{SO}_4^{2-}\right]$, (8)

6   Previous studies found that observed ammonium-sulfate aerosol molar ratio is lower than

7   2 over the US (Silvern et al., 2017; Hidy et al., 2014). Guo et al. (2018) found ammonium-sulfate

8   aerosol molar ratio during the Wintertime Investigation of Transport, Emissions, and Reactivity

9   (WINTER) study to be 1.47±0.43 and pointed out that this phenomena indicates an important

10   role of soluble nonvolatile cations in aerosol thermodynamics. To reflect the impact of soluble

11   nonvolatile cations on cloud water pH, we assume that total amount of soluble nonvolatile

12   cations associated with aerosol thermodynamics (SNVC) is 25% of sulfate. We also consider the

13   contribution of calcium and magnesium based on simulated dust mass in GC12, assuming that 3%

14   of dust mass is soluble calcium and 0.6% is soluble magnesium (Farlie et al., 2010; Moch et al.,

15   2020) , to soluble nonvolatile ions (SNVI):

16   $[\text{SNVI}] = 2\left[\text{SO}_4^{2-}\right] - 2[\text{SNVC}] - 2\left[\text{Ca}^{2+}\right] - 2\left[\text{Mg}^{2+}\right]$, (9)

17   Rainwater pH, which is used for the calculation of effective Henry's law constants of

18   water-soluble gases in rain droplets (Eqs. 3-5), is assumed to be a constant value of 4.5 in GC12.

19   Rainwater pH is determined by the cloud water pH where the rain is produced, uptake of water

20   and ions during rainfall processes, and evaporation of rain droplets. In addition, rainwater pH

21   also depends on temperature (Smith and Martell, 1976). Although it is difficult to fully trace

22   rainwater pH in the model based on current available information in GC12, we use cloud pH at

23   where rainout occurs to represent rainwater pH for rainout process and rainwater-mass-weighted

24   cloud pH above where washout occurs to represent rainfall water pH for washout process in this

25   work. The calculated rainwater pH in this study varied from 4.3 to 6.9.

26   pH values also affect dry deposition of water-soluble gases via its impact on the uptake

27   due to dissolution at wet surfaces. The origin of surface water where this uptake occurs is

28   therefore important to account for the effect if varying pH. GC12 calculated effective Henry's

29   constant for dry deposition by assuming temperature of 298.15 K and leaf water pH of 7. Surface

30   water on land is dominated by leaf water whose pH is ~7. The pH of ocean surface water varies

7

from 8 to 8.5 (Antonov, 2010; Jacobson, 2005). de Caritat et al. (2005) found the pH of the meltwaters of the Arctic snow varies from 4.6 to 6.1 with median value of 5.4. We assume the pH values at wet surface are 7 for land, 8.2 for ocean, and 5.4 for snow in this work.

2.2 Fraction of cloud available for aqueous phase chemistry

In GC12, the fraction of cloud available for aqueous phase chemistry is assumed to be 100% of grid box cloud fraction when temperatures are above 258 K and 0% of grid box cloud fraction when temperatures are below 258 K. This means aqueous phase chemistry in mixed clouds where temperatures are often below 258 K is not considered in GC12. However, many studies have indicated that supercooled cloud water can exist when temperatures are above 237 K (Rosenfeld and Woodley, 2000; Sassen, 1985). Therefore, we calculate aqueous phase cloud fraction based on MERRA-2 cloud liquid content and cloud ice content when temperatures are higher than 237 K:

$$f_{aq} = f_c \frac{\text{LCW}}{\text{LCW+ICW}}, \ (T > 237 \ \text{K}) \ , (10)$$

where f_{aq} is aqueous phase cloud fraction, LCW (g m^{-3}) is grid box mean liquid phase cloud water content, and ICW (g m^{-3}) is grid box mean ice phase cloud water content.

2.3 Rainout efficiencies
2.3.1 Warm cloud

GEOS-Chem uses rainout efficiencies to represent the absorptions of water-soluble gasses and aerosols in the cloud condensate phase (Jacob et al., 2000; Mari et al., 2000; Liu et al., 2001). After applying these efficiencies with the updated parameterization for rainout loss fraction (Luo et al., 2019), we get the new equation as

$$F = \frac{f_c \cdot P_r}{k\left(\text{LCW+ICW} + P_r \cdot \Delta t\right)}\left(1 - e^{-E_r \cdot k \cdot \Delta t}\right), (11)$$

where E_r is the rainout efficiency for corresponding species. Eq. (11) is the same as Eq. (1) except Eq. (11) contains E_r in the rainout calculation.

In GC12, rainout efficiencies for water-soluble aerosols are assumed to be 100% while those for water-soluble gases, except nitric acid and SO_2, are calculated via Henry's law constants (Jacob et al., 2000). E_r of nitric acid is assumed to be the same as water-soluble

aerosols due to its high solubility. E_r of SO_2 is assumed to be the same as water-soluble aerosols but limited by the availability of H_2O_2 in the precipitating grid box (Chin et al., 1996). It means rainout of SO_2 in GC12 is attribute to the aqueous phase oxidation of SO_2 by H_2O_2 rather than the absorption by cloud water. However, GEOS-Chem already accounted for in-cloud oxidation of SO_2 as part of the aqueous phase chemical calculation which converts in-cloud SO_2 to sulfate, so doing the same in the scavenging calculation would be double-counting the removal of SO_2. Considering the low solubility of SO_2 in water, it is more appropriate to calculate rainout efficiency for SO_2 based on Henry's law. In the present work, we assume E_r of SO_2 equals its dissolution fraction:

$$E_{r\_SO2} = f_{w\_SO2}, (12)$$

with f_{w_SO2} calculated with Eq. (2).

In the present work, we also modified rainout efficiencies for hydrophilic black carbon (BC) and primary organic carbon (POC), from 100% in GC12 to 50%. The rationale for the modification is that, although the aging of BC and POC in the atmosphere converts these aerosols from hydrophobic to hydrophilic, they are not as easily activated into cloud droplet as water-soluble aerosols (e.g. sulfate, nitrate, ammonium). The composition of the particles decides the hygroscopic parameter kappa which is important for cloud activation calculation (Abdul-Razzak et al., 2000). If BC and POC are internally mixed with the sulfate, nitrate, ammonium (SNA) aerosols, then they all have similar compositions. However, in the actual atmosphere, many particles are externally mixed: some particles are pure SNA while others are primary particles (BC, POC, dust, etc.) coated with SNA (Fassi-Fihri et al., 1997). It takes time for primary particles to gain coating through condensation, coagulation, and aqueous chemistry. The amount of SNA coated on primary particles depends on the aging time and abundance of SNA in the air. Based on a detailed size and mixing state resolved advanced particle microphysics (APM) simulation which explicitly resolves the amount of SNA coating (Yu et al., 2012), the hygroscopic parameter kappa of coated BC and POC is roughly about half of that of SNA. More robust calculation of rainout efficiencies for BC and POC should consider the amount of soluble species coated on these particles (Yu et al., 2012; Yu and Luo, 2009), but this will be the subject of future work.

2.3.2 Mixed and cold clouds

In GC12, aerosols in mixed clouds (237 K ≤ T < 258 K) and cold clouds (T < 237 K) were assumed to be removed through heterogeneous and homogeneous freezing nucleation (Wang et al., 2014). GEOS-Chem assumed that heterogeneous nucleation dominates ice formation at 237 K ≤ T < 258 K (mixed cloud) and results in 100% rainout efficiencies only for dust and hydrophobic black carbon which are considered as ice nuclei (IN). Homogeneous nucleation takes place at T < 237 K (cold cloud) and results in 100% rainout efficiencies for both water-soluble aerosol and IN.

Ice nucleation processes and their impacts on aerosol wet scavenging by mixed and cold clouds are largely unclear. However, it is known that ice nucleation rates depend strongly on temperature (DeMott et al., 2015; Kanji and Abbatt, 2010). To take into account this, we parameterize rainout efficiencies at warmer temperatures based on the fraction of dust in mixed clouds contributing to IN, which can be calculated as a function of T according to DeMott et al. (2015) as:

$$E_{r\_mixed\_dust} = \frac{e^{0.46(273.16-T)-11.6}}{153.5}, \ (237 \ K \le T < 258 \ K) \ , (13)$$

In addition to T, ice nucleation efficiency of particles also depends on their sizes and smaller particles (diameter < 500 nm) are less likely to act as IN (Niedermeier et al., 2015). While most of the mass of dust particles are dominated by those larger than 500 nm (Zender et al., 2003), a significant fraction of BC particles are smaller than 500 nm (Sahu et al., 2012). Based on sectional aerosol microphysics calculation in GEOS-Chem-APM (Yu and Luo, 2009), the mass fraction of BC particles with diameter > 500 nm is ~50%. In this study, we assume E_r for hydrophobic BC in both mixed cloud (237 K ≤ T < 258 K) and cold cloud (T < 237 K) are 50% of those values for dust.

Water-soluble aerosols are 100% removed via homogeneous freezing nucleation in cold cloud (Wang et al., 2014; Liu et al., 2001). Strom et al. (1997) observed that ~ 40% of preexisting aerosol mass is incorporated in ice crystals. In this work, we assume cold cloud rainout efficiencies are 40% for water-soluble aerosol, 50% for hydrophobic black carbon, and 100% for dust, respectively. Additionally, rainout of cold clouds is limited to below the MERRA-2 troposphere since stratospheric water in MERRA-2 is known to have unphysical behavior.

In GC12, cold cloud wet scavenging of nitric acid is treated the same as water-soluble aerosol. However, in cold clouds (T < 237 K), nitric acid is removed by the partitioning on ice crystals (Kärcher and Voigt, 2006; Voigt et al., 2006), while water-soluble aerosol is removed by homogeneous freezing nucleation. Kärcher et al. (2008) used a climatology of cirrus ice water content together with observed molar ratios of HNO_3/H_2O in cirrus ice particles to estimate the range of nitric acid content in cirrus ice (185-240 K). Their study showed that less efficient nitric acid uptake limits the nitric acid content in cirrus ice at higher temperatures and small ice water contents permit only little nitric acid in ice at low temperatures. The fraction of nitric acid in ice generally increases with decreasing temperature. Kärcher and Voigt (2006) attributed this behavior to less efficient nitric acid trapping at higher temperatures despite faster ice growth rates, which is caused by increasingly rapid escape of adsorbed nitric acid into the gas phase. A parameterization of nitric acid partitioning in cold cloud developed by Kärcher et al. (2008) is employed here to calculate E_r of nitric acid in cold cloud when temperature is below 240 K:

$$E_r = \frac{10^{-(-26.5 \times 1.00155^T + 30.7)} \cdot \frac{63}{18} \cdot [\frac{LCW + ICW}{f_c}]_{vmr}}{[HNO_3]_{vmr}} \ , (14)$$

where $[\frac{LCW + ICW}{f_c}]_{vmr}$ is volume mixing ratio of in-cloud water and in-cloud ice, and $[HNO_3]_{vmr}$ is volume mixing ration for nitric acid gas.

2.4 Empirical washout coefficients by rain and snow

Washout coefficients by rain and snow in GC12 were updated by Wang et al. (2011) by adopting the parameterization constructed by Feng (2007, 2009) for individual aerosol modes. Accumulation-mode washout coefficients were used for all aerosols except dust and sea salt, for which the coarse mode coefficients were used. Previous studies noticed that washout rates by rain derived from field measurements are 1 to 2 orders of magnitude larger than the values from theoretical calculation (Wang et al., 2010; Luo et al., 2019). Therefore, L2019 recommended using empirical washout coefficients for the simulation of washout by rain.

Wang et al. (2014) found that the large differences in washout rate between field measurements and theoretical calculation not only appear in washout by rain but also appear in washout by snow. In this work, we use the semi-empirical parameterization developed by Wang

1 et al. (2014) for the calculation of nitric acid and aerosol washout by both rain and snow.

2 Washout rate is calculated by an exponential equation:

3 $$k_{\text{wash}} = \Lambda \left(\frac{P_{\text{d}}}{f_{\text{r}}} \right)^b \ , (15)$$

4 where k_{wash} (s^{-1}) is the washout rate, P_{d} (mm h^{-1}) is rain or snow falling from upper layers, f_{r} is

5 rainfall area fraction, Λ is washout scavenging coefficient, and b is an exponential coefficient.

6   The values of Λ and b for nitric acid and aerosol washout by rain (T > 268 K) and snow

7 (248 K < T < 268 K) are shown in Table 1. We assume precipitation at temperatures lower than

8 248 K is dominated by ice. GC12 assumed washout of aerosol by ice is the same as that by snow.

9 However, uptake of aerosol by ice and by snow is different. Schneider et al. (2019) found

10 specific surface area (SSA) of ice crystal is ~1/5 of SSA of snow. Therefore, in this work, we

11 roughly assume washout rate by ice (T < 248 K) is 1/5 of that by snow. Washout of nitric acid

12 uses the same values as in L2019 but we extend the temperature limitation from 268 K to 248 K.

13 Washout of nitric acid by ice is assumed to be 1/5 of that by snow. Empirical washout

14 coefficients by rain and snow for coarse aerosol and hydrophobic fine aerosol in this work are

15 based on the values in Wang et al. (2014). Because the rain washout rate for water-soluble

16 aerosols measured by Laakso et al. (2003) is still ~ 20 times larger than that calculated by the

17 semi-empirical parameterization, we used the value of 1×10^{-5} to replace 5×10^{-7} for hydrophilic

18 aerosol's washout by rain. The washout coefficient of hydrophilic aerosol by snow is replaced

19 with the value of 2×10^{-4} which is 20 times higher than the value by rain. The assumption of

20 different washout coefficients for hydrophobic and hydrophilic aerosols is because the rain

21 washout rate for water-soluble aerosols measured by Laakso et al. (2003) is larger than that

22 calculated by the semi-empirical parameterization. One of the possible reasons is that droplet–

23 particle collection mechanisms for hydrophobic and hydrophilic aerosols are different. Washout

24 by ice is assumed to be 1/5 of that by snow.

25

26 **2.5 Wet surface uptake during dry deposition**

27   Uptake of water-soluble gases at wet surfaces is strongly influenced by dissolution

28 processes. The solubility of SO_2, H_2O_2, and NH_3 at wet surfaces needs to be calculated via

29 effective Henry's law coefficient because it is associated with a series of aqueous phase reactions

30 (Seinfeld and Pandis, 2016). In GC12, H^* of SO_2, H_2O_2, and NH_3 for dry deposition are assumed

1   to be the constants with the values of 10^5 M atm^{-1}, 5×10^7 M atm^{-1}, and 2×10^4 M atm^{-1},

2   respectively (http://wiki.seas.harvard.edu/geos-chem/index.php/Physical_properties_of_GEOS-

3   Chem_species#Definition_of_Henry.27s_law_constants). In this work, we consider the impacts

4   of temperature and pH at wet surface on the values of H^* (Erisman et al., 1994; Wesely et al.,

5   1990), and the values of H^* for SO_2, H_2O_2, and NH_3 are calculated with equations (3-5). Wet

6   surface pHs discussed in section 2.1 are used to reflect the impact of wet surface acidity on

7   dissolution during dry deposition. Wet surface pHs are only determined by land type and are not

8   altered by precipitation. Ganzeveld et al. (1998) reported that observations and physical-

9   chemical model simulations indicated SO_2 dry deposition velocity increases from a minimum

10   value of 0.01 cm s^{-1} for a temperature of 253 K to a value of 0.15-0.25 cm s^{-1} for 273 K.

11   Therefore, in this work, we assume SO_2 dry deposition velocity over snow and ice is 0.01 cm s^{-1}

12   when temperatures are lower than 253 K.

13

14   3. **Results and discussions**

15   To investigate the impacts of updated wet processes on global simulation of aerosols and

16   aerosol precursors, we run GEOS-Chem for 3 cases: (1) standard Geos-Chem version 12.6.0,

17   called GC12; (2) the same as case GC12 except using wet scavenging described in the work of

18   Luo et al. (2019), and this case is named L2019; (3) the same as the case L2019 except

19   considering the updated wet processes described in section 2, and this case is called WETrev. All

20   simulations are run with 2º×2.5º horizontal resolution and 47 layers from surface to 0.01 hPa.

21   Emission over Europe is based on the EMEP inventory. Other emissions are produced by the

22   default setting of HEMCO (Keller et al., 2014) for all simulations presented in this work.

23

24   **3.1 Comparison with surface monitoring networks over the US, Europe, and Asia**

25   To validate model results with surface monitoring networks, we use observational data

26   taken at USEPA, CASTNET, AMoN, IMPROVE and CSN, EMEP and EANET sites. The

27   criterion of observations used for model validation is that valid data are available for every

28   month in 2011. For EANET observations, due to too much missing data, the criterion is loosened

29   to monthly mean data available for each month during a 3-year period (2010-2012). Seto et al.

30   (2007) pointed out that EANET observations at urban sites are much higher than those at remote

31   sites. Since the number of the Asian sites is very limited, to make the validation more appropriate,

1   only remote and rural sites are used for model validation. Table 2 shows number of sites with

2   observations and number of sites satisfying these criteria. Figure 1 and Table 3 present the

3   comparisons of observed secondary inorganic aerosol precursors and secondary inorganic

4   aerosols at surface monitoring networks and the simulated mass concentrations by the GC12,

5   L2019, and WETrev cases described above. As shown in Fig. 1 (a-c), simulated SO_2 for the 3

6   cases is lower than observed values over the US but higher than the observations over Europe

7   and Asia. Over the US, simulated SO_2 is ~ 20% lower than observations. One possible reason is

8   that a large amount of USEPA observations are located at urban regions where SO_2

9   concentrations are much higher than rural and remote regions. There were 288 USEPA sites with

10 valid data in each month of 2011. Only 69 of these sites were with the mark of 'Not in a city'.

11 After considering the updates of wet scavenging by L2019, NMBs are increase from 20% to 23%

12 over the US, reduced from 74% to 59% over Europe, and reduced from 63% to 43% over Asia,

13 respectively. Considering of updated wet processes in this work further reduces NMBs to 51% in

14 Europe and 23% in Asia, respectively.

15   Figure 1 (d-f) are the results for nitric acid. NMBs of simulated nitric acid by GC12 for

16 the US, Europe, and Asia are 78%, 107%, and 121%, respectively. G12 significantly

17 overestimates surface mass concentration of nitric acid at these regions. Simulations by L2019

18 and WETrev indicate that wet scavenging is the dominant process causing the overestimation of

19 nitric acid in GEOS-Chem. NMBs of simulated nitric acid in WETrev for the US, Europe, and

20 Asia are reduced to 0.9%, -0.7%, and -21%, respectively. We also notice that WETrev

21 underestimates nitric acid at low temperatures for the US and Europe sites. These underestimates

22 may be associated with the updated uptake coefficients by Holmes et al. (2019) for

23 heterogeneous chemistry. If we switch back to the old heterogeneous chemistry in GEOS-Chem

24 version 12.5, the underestimation of nitric acid at low temperatures is reduced (not shown).

25 Figure 1 (g-i) show that the biases of model simulated ammonia by the 3 cases over the 3 regions

26 are small. Since the increasing ammonia wet deposition is compensated by less equilibrium

27 partitioning with decreased nitric acid in the air, wet processes show relatively small impact on

28 the simulation of ammonia.

29   Figure 1 (j-l) are observed and simulated sulfate over the US, Europe, and Asia. NMBs of

30 the GC12 case over the 3 regions are -1.1%, 6.9%, and 5.5%, respectively. The application of

31 updates to wet scavenging in L2019 leads to a significant underestimation of sulfate during

winter time, reaching up to 50% over the 3 regions. Based on our investigation, we found that the missing of aqueous phase chemistry in mixed cloud appears to be the main reason of underestimated sulfate at low temperatures. As we discussed in section 2, aqueous phase chemistry in GC12 is only simulated when temperatures are higher than 258 K. Conversely, in WETrev case, the temperature limitation of aqueous phase chemistry is extended from 258 K to 237 K. This change allows aqueous phase chemistry to be simulated when temperatures are low. After employing the new approaches of cloud water pH and aqueous phase cloud fraction calculation, NMBs of the WETrev case at the 3 regions are -10%, 4.3%, and 6.3%, respectively. It significantly reduces the bias shown in the L2019 case. The absence of aqueous phase hydroxymethanesulfonate chemistry may also be a potential reason for the remaining model biases with sulfate, but this is not explored here (Moch et al., 2018). NMB of sulfate simulated by WETrev in the US is higher than that of GC12. However, the good agreement between GC12 sulfate and the observation can be attributed to the coincidental offsets of the higher sulfate mass due to the underestimation of sulfate wet scavenging and the lower sulfate mass due to the absence of aqueous phase chemistry in mixed cloud and hydroxymethanesulfonate chemistry. As shown in Figure 1 (m-r), simulated nitrate and ammonium in the GC12 case over the 3 regions are much higher than observations. As discussed in Luo et al. (2019), the overestimation is associated with the underestimation of rainout and washout of nitric acid and nitrate. Updated wet scavenging in L2019 successfully reduces NMBs of nitrate over the 3 regions from 126% to 10%, 127% to 7.5%, and 269% to 47%, respectively. NMBs of ammonium over the 3 regions are reduced from 45% to -13%, 90% to -7.3%, and 167% to 42%, respectively. Updated wet processes in this work show relatively small impact on simulated nitrate and ammonium surface mass concentrations over the 3 regions.

   For simplicity, the WETrev case includes all updates to wet processes as described in Section 2. To understand the contribution of various updates to the overall changes in the predicted concentrations of aerosols and aerosol precursors, we carry out five numerical sensitivity study cases (RO, WO, RP, DD, and AC). RO case is the same as case WETrev except using rainout rate in GC12; WO case is the same as case WETrev except using washout rate in GC12; RP case is the same as case WETrev except assuming pH of rainwater for wet scavenging is 4.5; DD case is the same as case WETrev except using dry deposition treatment in GC12; and

15

1 AC case is the same as case WETrev except using aqueous phase chemistry treatment in GC12.

2 Relative contributions to the changes are calculated as:

3
$$RC_i = \frac{\sum\limits_{j=1}^{nsite}\left|C_{i,j}-C_{WETrev,j}\right|}{\sum\limits_{j=1}^{nsite}\left|C_{RO,j}-C_{WETrev,j}\right| + \sum\limits_{j=1}^{nsite}\left|C_{WO,j}-C_{WETrev,j}\right| + \sum\limits_{j=1}^{nsite}\left|C_{PR,j}-C_{WETrev,j}\right| + \sum\limits_{j=1}^{nsite}\left|C_{DD,j}-C_{WETrev,j}\right| + \sum\limits_{j=1}^{nsite}\left|C_{AC,j}-C_{WETrev,j}\right|} \, , (16)$$

4 where RC is the relative contribution (%), C is simulated surface mass concentration ($\mu g\ m^{-3}$), i

5 is the numerical sensitive study case index (e.g. when i=1, $C_{i,j}$ refers to $C_{RO,j}$), j is the site index.

6   Relative contributions of RO, WO, RP, DD, and AC to the changes of January and July

7 surface concentrations over the USA, Europe, and Asia sites are summarized in Table 4. In the

8 US, the changes of SO_2 are mainly caused by DD and AC whose contributions are up to 54.2%

9 and 25.0% in January and 50.5% and 22.3% in July. Rainout and washout both show a relatively

10 small impact on the changes of SO_2. In contrast, rainout and washout are important to the

11 changes of nitric acid, sulfate, nitrate, and ammonium. The contribution of wet scavenging to the

12 changes of these species exceeds 50% in both January and July. For nitric acid, nitrate, and

13 ammonium, the contribution of wet scavenging can be as high as 70-90%. For sulfate, AC also

14 plays an important role with relative contributions in January and July of 29.5% and 17.5%,

15 which is comparable to the contributions of RO and WO. For ammonia, most of the changes are

16 caused by DD and AC, with the sum of the 2 processes contributing > 50% of the changes. The

17 contribution of RP to SO_2, sulfate, ammonia, and ammonium is small in January and large in

18 July. In July the contribution of RP to SO_2, sulfate, ammonia, and ammonium is 8.5%, 4.4%,

19 13.4%, and 4.1%, respectively. The relative contribution from RO, WO, RP, DD, and AC at the

20 sites over Europe and Asia are similar to those over the US (Table 4).

21   Figure 2 is a comparison of observed BC and OC over the US and Europe. Simulated BC

22 over the US is close to observations except for a 10-20% underestimate during summer and fall.

23 The underestimate is likely associated with the underestimated wildfire emissions in the western

24 US (Mao et al., 2015). Simulated OC over the US is close to observations during summer but 50-

25 60% lower than observations during spring and fall. GEOS-Chem (all three cases) significantly

26 underestimates BC and OC over Europe and the possible reasons behind the bias remain to be

27 investigated. NMBs of the BC and OC in Europe are up to -37% and -61%, respectively. The

28 differences of simulated BC and OC in the 3 cases are small for the US and Europe which

29 indicates wet processes have a small impact on the simulation of BC and OC in these regions.

The small impact of wet processes on BC in the US and Europe is because 80% of emitted BC is assumed to be hydrophobic aerosol which needs 1.15 days to be converted to hydrophilic BC. Updated wet processes have little impact on hydrophobic aerosol in the lower troposphere where wet scavenging is dominated by warm clouds. OC consists of primary organic aerosol (POA) and SOA which is formed through the oxidation of organic gaseous precursors. Due to low dissolution of POA and organic gaseous precursors in water, wet processes also have little impact on these species.

Wet deposition of simulated SO_2+SO4, HNO_3+NIT, and NH_3+NH4 are compared with NTN observations over the US (Fig. 3), EMEP observations over Europe (Fig. 4), and EANET observations over remote region in Asia (Fig. 5). The criteria of observations used for model validation are (1) valid data are available for each month in 2011and (2) the difference between observed and simulated monthly precipitation is within a factor of 4 (Paulot et al., 2014). Number of sites with observations and number of sites satisfying these criteria are shown in Table 5. For the comparison shown in Table 6, model simulated wet depositions are corrected following Paulot et al. (2014) to remove bias due to precipitation. As shown in Figure 3 and Table 6, GC12 underestimates SO_2+SO4 wet deposition over the US and Europe. NMBs of SO_2+SO4 wet deposition simulated by GC12 over the two region are -21% and -46%, respectively. After considering the updated wet processes in WETrev, NMBs of SO_2+SO4 wet deposition are reduced to -9.0% over the US and -6.2% over Europe, respectively. However, all the three cases significantly underestimate SO_2+SO4 wet deposition over Asia. One possible reason is that GEOS-Chem may underestimate eruptive volcanic emission nearby the four Japanese sites. For HNO_3+NIT wet deposition over the US, the values simulated by GC12 are close to observations, while the values simulated by WETrev are ~ 2 times higher than observations. However, wet deposition data are collected weekly at NTN sites. It is hard to estimate the uncertainty due to the evaporation of HNO3 from the collected precipitation water. Over Europe and Asia, wet deposition fluxes are observed daily at most of EMEP and EANET sites. The values of HNO_3+NIT wet deposition simulated by GC12 are lower than observations, while the values simulated by WETrev are higher than observations. For NH_3+NH4, GC12 underestimates wet deposition over the US, Europe, and Asia. NMBs over the 3 regions are -10%, -33%, and -10%, respectively. NMBs of NH_3+NH4 wet deposition simulated by WETrev are reduced to -7.7% over Europe and -2.5% over Asia, respectively.

17

3.2 Comparison of SO₂, sulfate and BC mass concentrations at Arctic sites

We also study the impact of updated wet processes on SO_2, sulfate and BC surface mass concentrations at several Arctic sites where measurements are available. Figure 6 shows the comparison of SO_2 at Nord (81.6ºN, 16.7ºW) and Zeppelin (78.9ºN, 11.9ºE). GC12 matches well with the observed SO_2 at Nord but overestimates SO_2 at Zeppelin in January and December by a factor of 3. The updated wet scavenging (yellow line) shows a small impact on simulated SO_2 in the Arctic., with simulated SO_2 reduced slightly during winter and spring. In WETrev, we assumed SO_2 dry deposition velocity is 0.01 cm s^{-1} when temperatures are lower than 253 K. WETrev slightly enhances SO_2 at the higher latitude site Nord during winter. At Zeppelin, temperature in December is higher than that in January and February, and SO_2 concentration is enhanced due to the modification of dry deposition in this work. However, there is more aqueous phase chemistry in December which consumes the enhanced SO_2. By switching from GC12 to WETrev, NMB of SO_2 is increased from -23% to 32% at Nord and decreased from 27% to 22% at Zeppelin. Figure 7 compares the observed and simulated sulfate and BC at Alert (82.5ºN, 62.5ºW), Barrow (71.3ºN, 156.6ºW), and Zeppelin. Observations at the three sites show that both sulfate and BC are high in spring and low in summer. The model simulations generally capture seasonal variation at these Arctic sites. However, GC12 overestimates sulfate mass concentration at the 3 sites by a factor of 2-3. Simulated BC by GC12 is 50% lower than observation at Alert during winter and spring and a factor of 2 higher than observations at Barrow and Zeppelin during winter. Updated wet scavenging significantly impacts simulated sulfate and BC in Arctic regions. Simulated sulfate by L2019 is much closer to observations except for a 50% underestimation at Alert during winter and spring, while simulated BCs at the 3 Arctic sites by L2019 is much lower than observations. The comparison with model results from WETrev shows the underestimation of sulfate at Alert during spring is compensated by considering aqueous phase chemistry in mixed clouds. Most of BC at Arctic regions is transported from middle-low latitude source regions with open fire and anthropogenic emissions (Xu et al., 2017), and during the long-range transport hydrophobic BC is aged and converted to hydrophilic BC. The assumption of reduced hydrophilic BC rainout efficiency in the WETrev case increases simulated BC mass concentration and enhances agreement with observations at these Arctic sites.

1　NMBs of BC are reduced from -67% to -40% at Barrow and from -75% to -46% at Zeppelin due

2　to the switch from L2019 to WETrev.

3

4　**3.3 Vertical profiles of nitric acid and aerosols: Comparison with ATom-1 and ATom-2**

5　**aircraft measurements**

6　　　To evaluate the impact of updated wet processes on simulated vertical profiles of aerosols

7　and aerosol precursors, we compare simulated nitric acid and aerosols for the 3 cases with the

8　aircraft measurements of ATom-1 in July-August 2016 and ATom-2 in January-February 2017

9　(Jimenez et al., 2019; Wofsy et al., 2018) over the Northern Hemisphere (Fig. 8) and the

10　Southern Hemisphere (Fig. 9). Nitric acid was measured by Chemical Ionization Mass

11　Spectrometer, while aerosols were measured by CU Aircraft High-Resolution Time-of-Flight

12　Aerosol Mass Spectrometer (Hodzic et al., 2020). The work of Brock et al. (2019) indicated that

13　there is very good quantitative agreement between AMS and volume data. For ATom data, OC is

14　calculated by OA_PM1_AMS/OAtoOC_PM1_AMS. For model, we used 1.8 for SOAs. Flight

15　tracks over the land or in the stratosphere are filtered out for the comparison (see Figure S1 in

16　supporting materials for flight tracks of ATom-1 amd ATom-2). We filter out the flight tracks

17　over the land is because ATom observations over the land, whose values vary greatly, only

18　account for 28% of total measurements. The exclusion of these data makes the comparison more

19　appropriate. Vertical profiles of nitric acid and aerosols over the land, which are similar to Fig. 8

20　and 9, are shown in Figure S2.

21　　　As shown in Figure 8, GC12 overestimates nitric acid and underestimates black carbon

22　and organic carbon over the Northern Hemisphere during both ATom-1 and ATom-2. NMBs of

23　the 3 species are 66%, -77%, and -55% during ATom-1 and 163%, -10%, and -27% during

24　ATom-2. GC12 simulated sulfate and ammonium match well with observations during ATom-1

25　but are much higher than observations during ATom-2 whose values are high up to 78% for

26　sulfate and 217% for ammonium. After considering the updated wet scavenging in L2019, the

27　overestimates of nitric acid, sulfate, and ammonium during ATom-2 and nitric acid during

28　ATom-1 are reduced to 5%, -11%, -30%, and -36%, respectively. However, L2019 significantly

29　underestimates nitric acid at the upper troposphere where pressure is lower than 300 hPa. As we

30　mentioned earlier, L2019 may overestimate cold cloud wet scavenging of nitric acid due to

31　treatment of cold cloud rainout of nitric acid as same as water-soluble aerosol with 100% rainout

efficiency. With updated cold cloud scavenging in WETrev, the bias of nitric acid simulated by L2019 at the upper troposphere is reduced during ATom-2 and is enhanced during ATom-1. This indicates further understanding regarding ice uptake and removal of nitric acid are needed. Nitric acid concentrations simulated by WETrev between 500 hPa and 300 hPa are much lower than those simulated by L2019 and GC12. This is because WETrev considers washouts of nitric acid by snow and ice which were absent in L2019 and GC12. Figure 8 (g) shows the impact of updated aqueous phase chemistry in mixed clouds on the sulfate vertical profile. Considering aqueous phase chemistry in mixed clouds significantly enhances sulfate mass concentration within the range of 700-500 hPa during ATom-2 which makes the simulated sulfate much closer to observed values. Figures 8 (d) and (i) indicate that the impact of updated wet scavenging on the black carbon vertical profile during ATom-2 is more obvious than that during ATom-1. This is because there is much less black carbon emitted from open fires in January than there is in July. Black carbon observed during ATom-2 is dominated by hydrophilic black carbon which is more affected by wet scavenging processes, while black carbon observed during ATom-1 is dominated by hydrophobic black carbon. Updated wet scavenging shows a small impact on organic carbon vertical profiles during both ATom-1 and ATom-2. Figure 9 shows comparisons over the Southern Hemisphere. Updated wet scavenging reduces overestimated nitric acid especially during ATom-1 period. NMB is reduced from 80% to -25%. For sulfate, ammonium, black carbon, and organic carbon, the differences among the 3 cases are relative small. NMBs of WETrev for these species are larger than those of GC12. All cases significantly underestimate black carbon from open fire and organic carbon in the upper troposphere. Based on the comparisons with ATom-1 and ATom-2 measurements, it is clear that the updated wet process treatments in this work and L2019 can improve the agreements of simulated and observed vertical profiles of nitric acid (Fig. 8a, Fig. 8f, Fig. 9a, and Fig. 9f). The simulated of winter time sulfate and ammonium in the Northern Hemisphere are also improved by WETrev.

3.4 Impact on global distributions of surface mass concentrations

The impacts of updated wet process treatments on global simulation of surface mass concentrations are shown in Figures 10-14. Figures 10-12 show simulated surface mass concentrations of secondary inorganic aerosol precursors (SO_2, nitric acid, and ammonia), secondary inorganic aerosols (sulfate, nitrate, and ammonium), primary inorganic aerosols (sea-

salt, dust, and black carbon), and organic carbon (primary organic aerosol and secondary organic aerosol) simulated by GC12 case and WETrev case, while figures 13-14 are the percentage differences.

As shown in Figure 10, high values of secondary inorganic aerosol precursors are mainly located over continental regions with high anthropogenic and natural emissions. After considering the updated wet process treatments in this study, global mean surface mass concentrations (GMSMC) of SO_2, nitric acid, and ammonia are changed from 0.73 μg m^{-3}, 0.56 μg m^{-3}, 0.32 μg m^{-3} to 0.75 μg m^{-3}, 0.26 μg m^{-3}, 0.42 μg m^{-3}, respectively. The updated wet process treatments slightly impact GMSMC of SO_2 but strongly impact GMSMC of nitric acid. The impact on ammonia is small over land but large over ocean. The weak impact of the updated wet process treatments on SO_2 is because its wet removal is dominated by aqueous phase chemistry. The strong impact of the updated wet process treatments on ammonia over ocean is due to the changes of rainwater pHs over remote regions whose values are higher than the assumed 4.5 rainwater pH in GC12. Some large changes of surface mass concentration at Arctic and Antarctic regions, as shown in Figure 13 (a-c), are associated with the updated treatments of wet surface uptake during dry deposition at snow and ice. However, due to low mass concentrations for Arctic and Antarctic regions, their impacts on GMSMC are small. The updated wet process treatments significantly impact GMSMC of secondary inorganic aerosols whose water solubility is high. After considering the updated wet process treatments, GMSMC of sulfate, nitrate, and ammonium are changed from 0.84 μg m^{-3}, 0.42 μg m^{-3}, 0.33 μg m^{-3} to 0.74 μg m^{-3}, 0.21 μg m^{-3}, 0.26 μg m^{-3}, respectively. Their global mean relative changes are high up to -25%, -53%, and -22%, respectively. Most of the reductions of these species happen at middle-high latitude regions with high mass concentrations.

Figures 12 and 14 show the impact of updated wet process treatments on primary inorganic aerosols and organic carbon. It is clear that the updated wet process treatments have little impact on GMSMCs of these species. For sea salt, its high concentrations are mainly located at middle latitude regions in both the Northern Hemisphere and Southern Hemisphere where in cloud condensation water values are close to the assumed constant value in GC12. Therefore, the differences of wet scavenging in GC12 and WETrev cases at these regions are small. For dust, due to its low water solubility, the updated wet processes show a small impact in the lower troposphere where wet scavenging is dominated by warm clouds. Most of black carbon

and organic carbon are emitted as hydrophobic aerosols and then converted to be hydrophilic aerosols due to aging. Therefore, the updated wet process treatments show only a small impact at source regions but show a strong impact for remote regions.

4. Summary

In this study, we updated aqueous phase chemistry and wet scavenging for SO_2 and sulfate, rainout efficiencies for warm, mixed, and cold clouds, empirical washout by rain and snow, and wet surface uptake during dry deposition in GEOS-Chem version 12.6.0. Systematic validations of simulated aerosols and aerosol precursors with ground based monitoring networks over the US, Europe, and Asia, in-site observations at Arctic for surface mass concentrations and aircraft measurements during ATom-1 and ATom2 for their vertical profiles were presented. Based on these validations, we found:

(1) The model results with the updated treatment of wet processes agree better with measurements for most species in different regions, especially for nitric acid, nitrate, and ammonium whose NMBs were improved, respectively, from 78%, 126%, and 45% to 0.9%, 15%, and 4.1% over US sites, from 107%, 127%, and 90% to -0.7%, 4.2%, and 16% over Europe sites, and from 121%, 269%, and 167% to -21%, 37%, and 86% over Asia remote region sites;

(2) Comparing to Luo et al. (2019), the updated aqueous phase chemistry and wet scavenging of SO_2 and sulfate significantly improve the agreement of simulated SO_2 and sulfate over the US, Europe and Asia remote region, especially during the winter time. NMBs of sulfate in the 3 regions are reduced from -30%, -33%, and -36% to -10%, 4.3%, and 6.3%;

(3) The updated wet process treatments significantly improve the performance of sulfate wet deposition simulation over the US and Europe. NMBs are reduced from -35% to -9% over the US and from -46% to -6.2% over Europe, respectively;

(4) The updated rainout efficiencies enhance BC mass concentration for remote regions and successfully reduce the bias between simulation and observation at Arctic sites. NMBs of BC are reduced from -67% to -40% at Barrow and from -75% to -46% at Zeppelin due to the switch from L2019 to WETrev;

(5) Cold cloud scavenging plays important roles in the simulation at the upper troposphere, especially for nitric acid.

(6) The updated wet surface uptake during dry deposition changes the performance of simulated SO_2 at Arctic sites. NMB of SO_2 is increased from -23% to 32% at Nord and decreased from 27% to 22% at Zeppelin.

Wet processes are important for atmospheric chemistry modeling. Our study indicates that the updated wet process treatments introduced in this study have strong impacts on global means of water soluble aerosols and aerosol precursors such as nitric acid, sulfate, nitrate, and ammonium. The updated wet process treatments exhibit relatively small impacts on the simulated global means of SO_2, dust, sea salt, black carbon, and organic carbon. Although there are clear improvements derived from the updated treatment of wet processes, there still exist limitations of the work presented in this study. For example, washout efficiencies of water soluble species such as SO_2 and ammonia are sensitive to rain water pH values. In this study, we simply assumed rainwater pHs for rainout and washout are cloud pH at where rainout occurs and rainwater-mass-weighted cloud pH above where washout occurs, respectively. However, rain water pH needs to be calculated by tracing the cloud process and precipitation process of rain water lifecycle. The impact of traced rain water pH on wet scavenging needs to be further investigated.

Code and data availability. The code of GEOS-Chem 12.6.0 is available through the GEOS-Chem distribution web-page http://wiki.seas.harvard.edu/geos-chem/index.php/GEOS-Chem_12. The updated wet process code can be obtained by contacting the author directly. All measurement data are publicly available. USEPA data are download from https://www.epa.gov/outdoor-air-quality-data; CASTNET, AMon, IMPROVE, CSN data are download from http://views.cira.colostate.edu/fed/; NTN data are download from http://nadp.slh.wisc.edu/data/ntn/ntnAllsites.aspx; EMEP date are download from http://ebas.nilu.no/default.aspx and https://projects.nilu.no//ccc/emepdata.html; EANET data are download from https://monitoring.eanet.asia/document/signin; ATom data are download from https://espoarchive.nasa.gov/archive/browse/atom.

References

Abdul-Razzak, H., and Ghan, S. J., A parameterization of aerosol activation: 2. Multiple aerosol types, J. Geophys. Res., 105(D5), 6837– 6844, doi:10.1029/1999JD901161, 2000.

Alexander, B., D.J. Allman, H.M. Amos, T.D. Fairlie, J. Dachs, D.A. Hegg and R.S. Sletten, Isotopic constraints on sulfate aerosol formation pathways in the marine boundary layer of the subtropical northeast Atlantic Ocean, J. Geophys. Res., 117, D06304, doi:10.1029/2011JD016773, 2012.

Amos, H. M., Jacob, D. J., Holmes, C. D., Fisher, J. A., Wang,Q., Yantosca, R. M., Corbitt, E. S., Galarneau, E., Rutter, A. P.,Gustin, M. S., Steffen, A., Schauer, J. J., Graydon, J. A., Louis,V. L. St., Talbot, R. W., Edgerton, E. S., Zhang, Y., and Sunder-land, E. M.: Gas-particle partitioning of atmospheric Hg(II) and its effect on global mercury deposition, Atmos. Chem. Phys., 12,591–603, https://doi.org/10.5194/acp-12-591-2012, 2012.

Antonov JI, Seidov D, Boyer TP, Locarnini RA, Mishonov AV,Garcia HE, Baranova OK, Zweng MM, Johnson DR: World Ocean Atlas 2009, Volume 2: Salinity. In: Levitus S (ed)NOAA Atlas NESDIS 69, US Government Printing Office, Washington, 2010.

Bey, I., Jacob, D. J., Yantosca, R. M., Logan, J. A., Field, B. D., Fiore, A. M., Li, Q., Liu, H. Y., Mickley, L. J., and Schultz, M. G.: Global modeling of tropospheric chemistry with assimilated meteorology: Model description and evaluation, J. Geophys. Res., 106(D19), 23073– 23095, doi:10.1029/2001JD000807, 2001.

Brock, C. A., Williamson, C., Kupc, A., Froyd, K. D., Erdesz, F., Wagner, N., Richardson, M., Schwarz, J. P., Gao, R.-S., Katich, J. M., Campuzano-Jost, P., Nault, B. A., Schroder, J. C., Jimenez, J. L., Weinzierl, B., Dollner, M., Bui, T., and Murphy, D. M.: Aerosol size distributions during the Atmospheric Tomography Mission (ATom): methods, uncertainties, and data products, Atmos. Meas. Tech., 12, 3081–3099, https://doi.org/10.5194/amt-12-3081-2019, 2019.

Chin, M., Jacob, D. J., Gardner, G. M., Foreman‐Fowler, M. S., Spiro, P. A., and Savoie, D. L.: A global three‐dimensional model of tropospheric sulfate, J. Geophys. Res., 101(D13), 18667– 18690, doi:10.1029/96JD01221, 1996.

Chin, M., R. B. Rood, S.-J. Lin, J.-F. Muller, and A. M. Thompson: Atmospheric sulfur cycle simulated in the global modelGOCART: Model description and global properties.J. Geophys.Res.,105,24 671–24 687, 2000.

de Caritat, P., Hall, G., Gislason, S., Belsey, W., Braun, M.,Goloubeva, N. I., Olsen, H. K., Scheie, J. O., and Vaive, J. E.: Chemical composition of arctic snow: concentration level andregional distribution of major elements, Sci. Total Environ., 336,183–199, 2005.

DeMott, P. J., Prenni, A. J., McMeeking, G. R., Sullivan, R. C., Petters, M. D., Tobo, Y., Niemand, M., Möhler, O., Snider, J. R., Wang, Z., and Kreidenweis, S. M.: Integrating laboratory and field data to quantify the immersion freezing ice nucleation activity of

mineral dust particles, Atmos. Chem. Phys., 15, 393–409, https://doi.org/10.5194/acp-15-393-2015, 2015.

Erisman, J. W., Van Pul, A., and Wyers, G. P.: Parameterizationof surface resistance for the quantification of atmospheric deposition of acidifying pollutants and ozone, Atmos. Environ., 28,2595–2607, 1994.

Ervens, B., Turpin, B. J., and Weber, R. J.: Secondary organic aerosol formation in cloud droplets and aqueous particles (aqSOA): a review of laboratory, field and model studies, Atmos. Chem. Phys., 11, 11069–11102, https://doi.org/10.5194/acp-11-11069-2011, 2011.

Fairlie, T. D., Jacob, D. J., Dibb, J. E., Alexander, B., Avery, M. A., van Donkelaar, A. and Zhang, L.: Impact of mineral dust on nitrate, sulfate, and ozone in transpacific Asian pollution plumes, Atmos. Chem. Phys., 10(8), 3999–4012, doi:10.5194/acp-10-3999-2010, 2010.

Fassi-Fihri, A., Suhre, K., and Rosset, R.: Internal and external mixing in atmospheric aerosols by coagulation: impact on the optical and hygroscopic properties of the sulphate-soot system, Atmos. Environ., 10, 1393–1402, 1997.

Feng, J.: A 3-mode parameterization of below-cloud scavenging ofaerosols for use in atmospheric dispersion models, Atmos. Environ., 41, 6808–6822, 2007.

Feng, J.: A size-resolved model for below-cloud scavenging of aerosols by snowfall, J. Geophys. Res.-Atmos., 114, D08203, doi:10.1029/2008JD011012, 2009.

Ganzeveld, L., Lelieveld, J., and Roelofs, G. ‑ J.: A dry deposition parameterization for sulfur oxides in a chemistry and general circulation model, J. Geophys. Res., 103(D5), 5679–5694, doi:10.1029/97JD03077, 1998.

Garland, J.A. and Branson, J.R.: The deposition of sulphur dioxide to pine forest assessed by a radioactive tracer method. Tellus, 29: 445-454. doi:10.1111/j.2153-3490.1977.tb00755.x, 1977.

Guo, H., Nenes, A., and Weber, R. J.: The underappreciated role of nonvolatile cations in aerosol ammonium-sulfate molar ratios, Atmos. Chem. Phys., 18, 17307–17323, https://doi.org/10.5194/acp-18-17307-2018, 2018.

Hodzic, A., Campuzano-Jost, P., Bian, H., Chin, M., Colarco, P. R., Day, D. A., Froyd, K. D., Heinold, B., Jo, D. S., Katich, J. M., Kodros, J. K., Nault, B. A., Pierce, J. R., Ray, E.,

Schacht, J., Schill, G. P., Schroder, J. C., Schwarz, J. P., Sueper, D. T., Tegen, I., Tilmes, S., Tsigaridis, K., Yu, P., and Jimenez, J. L.: Characterization of organic aerosol across the global remote troposphere: a comparison of ATom measurements and global chemistry models, Atmos. Chem. Phys., 20, 4607–4635, https://doi.org/10.5194/acp-20-4607-2020, 2020.

Henzing, J. S., Olivié, D. J. L., and van Velthoven, P. F. J.:A parameterization of size resolved below cloud scaveng-ing of aerosols by rain, Atmos. Chem. Phys., 6, 3363–3375,https://doi.org/10.5194/acp-6-3363-2006, 2006.

Hidy, G. M., Blanchard, C. L., Baumann, K., Edgerton, E., Tanenbaum, S., Shaw, S., Knipping, E., Tombach, I., Jansen, J., and Walters, J.: Chemical climatology of the southeastern United States, 1999–2013, Atmos. Chem. Phys., 14, 11893–11914, https://doi.org/10.5194/acp-14-11893-2014, 2014.

Holmes, C. D., Bertram, T. H., Confer, K. L., Graham, K. A., Ronan, A. C., Wirks, C. K., & Shah, V.: The role of clouds in the tropospheric NOx cycle: A new modeling approach for cloud chemistry and its global implications. Geophysical Research Letters, 46, 4980–4990. https://doi.org/10.1029/2019GL081990, 2019.

Hopke, P.K., Ito, K., Mar, T., Christensen, W.F., Eatough, D.J., Henry, R.C., Kim, E., Laden, F., Lall, R., Larson, T.V., Liu, H., Neas, L., Pinto, J., St€olzel, M., Suh, H., Paatero, P., Thurston, G.D.: PM source apportionment and health effects: 1. Intercomparison of source apportionment results. J. Expo. Sci. Environ. Epidemiol. 16, 275e286, 2006.

Jacob, D. J., Liu, H., Mari, C., and Yantosca, B. M., Harvard wet de-position scheme for GMI, available at: http://acmg.seas.harvard.edu/geos/wiki_docs/deposition/wetdep.jacob_etal_2000.pdf (last access: December 2019), 2000.

Jacobson, M. Z.: Studying ocean acidification with conservative, stable numerical schemes for nonequilibrium air‐ocean exchange and ocean equilibrium chemistry, J. Geophys. Res., 110, D07302, doi:10.1029/2004JD005220, 2005.

Jimenez, J.L., P. Campuzano-Jost, D.A. Day, B.A. Nault, D.J. Price, and J.C. Schroder, ATom: L2 Measurements from CU High-Resolution Aerosol Mass Spectrometer (HR-AMS). ORNL DAAC, Oak Ridge, Tennessee, USA. https://doi.org/10.3334/ORNLDAAC/1716, 2019.

Kanji, Z. A., and J. P. D. Abbatt: Ice nucleation onto Arizona test dust at cirrustemperatures: Effect of temperature and aerosol size on onsetrelative humidity.J. Phys. Chem.,114A, 935–941, 2010.

Kärcher, B., and Voigt, C.: Formation of nitric acid/water ice particles in cirrus clouds, Geophys. Res. Lett., 33, L08806, doi:10.1029/2006GL025927, 2006.

Kärcher, B., M., C. Schiller, C. Voigt, H. Schlager, and P. Popp: A climatological view to HNO3 partitioning in cirrus clouds, Q. J. R. Meteorol. Soc., 134, 905–912, doi:10.1002/qj.253, 2008.

Keller, C. A., Long, M. S., Yantosca, R. M., Da Silva, A. M., Pawson, S., and Jacob, D. J.: HEMCO v1.0: a versatile, ESMF-compliant component for calculating emissions in atmospheric models, Geosci. Model Dev., 7, 1409–1417, https://doi.org/10.5194/gmd-7-1409-2014, 2014.

Kinne, S., Schulz, M., Textor, C., Guibert, S., Balkanski, Y., Bauer, S. E., Berntsen, T., Berglen, T. F., Boucher, O., Chin, M., Collins, W., Dentener, F., Diehl, T., Easter, R., Feichter, J., Fillmore, D., Ghan, S., Ginoux, P., Gong, S., Grini, A., Hendricks, J., Herzog, M., Horowitz, L., Isaksen, I., Iversen, T., Kirkevåg, A., Kloster, S., Koch, D., Kristjansson, J. E., Krol, M., Lauer, A., Lamarque, J. F., Lesins, G., Liu, X., Lohmann, U., Montanaro, V., Myhre, G., Penner, J., Pitari, G., Reddy, S., Seland, O., Stier, P., Takemura, T., and Tie, X.: An AeroCom initial assessment – optical properties in aerosol component modules of global models, Atmos. Chem. Phys., 6, 1815–1834, https://doi.org/10.5194/acp-6-1815-2006, 2006.

Laakso, L., Grönholm, T., Rannik, U., Kosmale, M., Fiedler, V.,Vehkamäki, H., and Kulmala, M.: Ultrafine particle scavenging coefficients calculated from 6 years field measurements, Atmos. Environ., 37, 3605–3613, 2003.

Liu, H. Y., Jacob, D. J., Bey, I., and Yantosca, R. M.: Constraints from Pb-210 and Be-7 on wet deposition and transport in a global three-dimensional chemical tracer model driven by as-similated meteorological fields, J. Geophys. Res.-Atmos., 106,12109–12128, 2001.

Luo, G., Yu, F., and Schwab, J.: Revised treatment of wet scavenging processes dramatically improves GEOS-Chem 12.0.0 simulations of surface nitric acid, nitrate, and ammonium over the United States, Geosci. Model Dev., 12, 3439–3447, https://doi.org/10.5194/gmd-12-3439-2019, 2019.

Mao, Y. H., Li, Q. B., Henze, D. K., Jiang, Z., Jones, D. B. A., Kopacz, M., He, C., Qi, L., Gao, M., Hao, W.-M., and Liou, K.-N.: Estimates of black carbon emissions in the western United States using the GEOS-Chem adjoint model, Atmos. Chem. Phys., 15, 7685–7702, https://doi.org/10.5194/acp-15-7685-2015, 2015.

Mari, C., Jacob, D. J., and Bechtold, P.: Transport and scavenging of soluble gases in a deep convective cloud, J. Geophys. Res., 105 (D17), 22255–22267, doi:10.1029/2000JD900211, 2000.

Martin, R. V., Jacob, D. J., Yantosca, R. M., Chin, M., and Ginoux, P.: Global and regional decreases in tropospheric oxidants from photochemical effects of aerosols, J. Geophys. Res., 108, 4097, doi:10.1029/2002JD002622, D3, 2003.

Moch, J. M., Dovrou, E., Mickley, L. J., Keutsch, F. N., Cheng, Y., Jacob, D. J., Jiang, J., Li, M., Munger, J. W., Qiao, X. and Zhang, Q.: Contribution of Hydroxymethane Sulfonate to Ambient Particulate Matter: A Potential Explanation for High Particulate Sulfur During Severe Winter Haze in Beijing, Geophysical Research Letters, 45(21), 11,969-11,979, doi:10.1029/2018GL079309, 2018.

Moch, J.M., E. Dovrou, L.J. Mickley, F.N. Keutsch, Z. Liu, Y. Wang, T.L. Dombek, M. Kuwata, S.H. Budisulistiorini, L. Yang, S. Decesari, M. Paglione, B. Alexander, J. Shao, J.W. Munger, D.J. Jacob, Global importance of hydroxymethanesulfonate in ambient particular matter: Implications for air quality, submitted to J. Geophys. Res., 2020.

Myhre, G., Samset, B. H., Schulz, M., Balkanski, Y., Bauer, S., Berntsen, T. K., Bian, H., Bellouin, N., Chin, M., Diehl, T., Easter, R. C., Feichter, J., Ghan, S. J., Hauglustaine, D., Iversen, T., Kinne, S., Kirkevåg, A., Lamarque, J.-F., Lin, G., Liu, X., Lund, M. T., Luo, G., Ma, X., van Noije, T., Penner, J. E., Rasch, P. J., Ruiz, A., Seland, Ø., Skeie, R. B., Stier, P., Takemura, T., Tsigaridis, K., Wang, P., Wang, Z., Xu, L., Yu, H., Yu, F., Yoon, J.-H., Zhang, K., Zhang, H., and Zhou, C.: Radiative forcing of the direct aerosol effect from AeroCom Phase II simulations, Atmos. Chem. Phys., 13, 1853–1877, https://doi.org/10.5194/acp-13-1853-2013, 2013.

Niedermeier, D., S. Augustin-Bauditz, S. Hartmann, H. Wex, K. Ignatius, and F. Stratmann: Can we define an asymptotic value for theice active surface site density for heterogeneous ice nucleation? J. Geophys. Res. Atmos., 120, 5036–5046, doi:10.1002/2014JD022814, 2015.

Pandis, S. N., and Seinfeld, J. H.: Sensitivity analysis of a chemical mechanism for aqueous‐phase atmospheric chemistry, J. Geophys. Res., 94(D1), 1105– 1126, doi:10.1029/JD094iD01p01105, 1989.

Paulot, F., Jacob, D. J., Pinder, R. W., Bash, J. O., Travis, K., and Henze, D. K.: Ammonia emissions in the United States, European Union, and China derived by high‐resolution inversion of ammonium wet deposition data: Interpretation with a new agricultural emissions inventory (MASAGE_NH3), J. Geophys. Res. Atmos., 119, 4343– 4364, doi:10.1002/2013JD021130, 2014.

Penner, J.E., R.J. Charlson, J.M. Hales, N.S. Laulainen, R. Leifer, T. Novakov, J. Ogren, L.F. Radke, S.E. Schwartz, and L. Travis: Quantifying and Minimizing Uncertainty of Climate Forcing by Anthropogenic Aerosols. Bull. Amer. Meteor. Soc., 75, 375–400, https://doi.org/10.1175/1520-0477(1994)075<0375:QAMUOC>2.0.CO;2, 1994

Rosenfeld, D., W.L. Woodley: Deep convective clouds with sustained highly supercooled liquid water until -37.5øC. Nature, 405,440-442, 2000.

Sassen, K.: Supercooled Liquid Water In Winter Storms: A Preliminary Climatology from Remote Sensing Observations, J. Wea. Mod., 17, 30-35, 1985.

Schneider, A., Flanner, M., De Roo, R., and Adolph, A.: Monitoring of snow surface near-infrared bidirectional reflectance factors with added light-absorbing particles, The Cryosphere, 13, 1753–1766, https://doi.org/10.5194/tc-13-1753-2019, 2019.

Seinfeld, J.H. and Pandis, S.N.: Atmospheric Chemistry and Physics: From Air Pollution to Climate Change. John Wiley & Sons, Hoboken, 2016.

Shiraiwa, M., Ueda, K., Pozzer, A., Lammel, G., Kampf, C. J.,Fushimi, A., Enami, S., Arangio, A. M., Fröhlich-Nowoisky, J.,Fujitani, Y., Furuyama, A., Lakey, P. S. J., Lelieveld, J., Lucas,K., Morino, Y., Pöschl, U., Takahama, S., Takami, A., Tong, H.,Weber, B., Yoshino, A., and Sato, K.: Aerosol Health Effectsfrom Molecular to Global Scales, Environ. Sci. Technol., 51, 13545–13567, https://doi.org/10.1021/acs.est.7b04417, 2017.

Silvern, R. F., Jacob, D. J., Kim, P. S., Marais, E. A., Turner, J. R., Campuzano-Jost, P., and Jimenez, J. L.: Inconsistency of ammonium–sulfate aerosol ratios with thermodynamic models in the eastern US: a possible role of organic aerosol, Atmos. Chem. Phys., 17, 5107–5118, https://doi.org/10.5194/acp-17-5107-2017, 2017.

Smith, R.M. and Martell, A.E.: Critical Stability Constants, Vol. 2, Amine Complexes, Plenum Publ., Co., New York, 1976.

Strom, J., B. Strauss, T. Anderson, F. Schroder, J. Heintzenberg, and P. Wendhng: In situ observations of the microphysical properties of young cirrus clouds, J. Atmos. Sci., 541, 2542-2553, 1997.

Sahu, L. K., Y. Kondo, N. Moteki, N. Takegawa, Y. Zhao, M. J. Cubison, J. L. Jimenez, S. Vay, G. S. Diskin, A. Wisthaler, T. Mikoviny, L. G. Huey, A. J. Weinheimer, D. J. Knapp, Emission characteristics of black carbon in anthropogenic and biomass burning plumes over California during ARCTAS‐CARB 2008, J. Geophys. Res., 117, D16302, doi:10.1029/2011JD017401, 2012.

Seto, S., Sato, M., Tatano, T., Kusakari, T. and Hara, H., Spatial distribution and source identification of wet deposition at remote EANET sites in Japan. Atmos. Environ.41,9386-9396, 2007.

Textor, C., Schulz, M., Guibert, S., Kinne, S., Balkanski, Y., Bauer, S., Berntsen, T., Berglen, T., Boucher, O., Chin, M., Dentener, F., Diehl, T., Easter, R., Feichter, H., Fillmore, D., Ghan, S., Ginoux, P., Gong, S., Grini, A., Hendricks, J., Horowitz, L., Huang, P., Isaksen, I., Iversen, I., Kloster, S., Koch, D., Kirkevåg, A., Kristjansson, J. E., Krol, M., Lauer, A., Lamarque, J. F., Liu, X., Montanaro, V., Myhre, G., Penner, J., Pitari, G., Reddy, S., Seland, Ø., Stier, P., Takemura, T., and Tie, X.: Analysis and quantification of the diversities of aerosol life cycles within AeroCom, Atmos. Chem. Phys., 6, 1777–1813, https://doi.org/10.5194/acp-6-1777-2006, 2006.

Turnock, S. T., Mann, G. W., Woodhouse, M. T., Dalvi, M., O'Connor, F. M., Carslaw, K. S., & Spracklen, D. V.: The impact of changes in cloud water pH on aerosol radiative forcing. Geophysical Research Letters, 46, 4039– 4048. https://doi.org/10.1029/2019GL082067, 2019.

Voigt, C., Schlager, H., Ziereis, H., K̈archer, B., Luo, B. P., Schiller,C., Kr̈amer, M., Popp, P. J., Irie, H., and Kondo, Y.: Nitric acidin cirrus clouds, Geophys. Res. Lett., 33, L05803, doi: 10.1029/2005GL025159, 2006.

Walcek, C.J. and G.R. Taylor: A Theoretical Method for Computing Vertical Distributions of Acidity and Sulfate Production within Cumulus Clouds. J. Atmos. Sci., 43, 339–355, https://doi.org/10.1175/1520-0469(1986)043<0339:ATMFCV>2.0.CO;2, 1986.

Wang, Q., Jacob, D. J., Fisher, J. A., Mao, J., Leibensperger, E. M.,Carouge, C. C., Le Sager, P., Kondo, Y., Jimenez, J. L., Cubi-son, M. J., and Doherty, S. J.: Sources of carbonaceous aerosolsand deposited black carbon in the Arctic in winter-spring: impli-cations for radiative forcing, Atmos. Chem. Phys., 11, 12453–12473, https://doi.org/10.5194/acp-11-12453-2011, 2011.

Wang, Q., Jacob, D. J., Spackman, J. R., Perring, A. E., Schwarz, J.P., Moteki, N., Marais, E. A., Ge, C., Wang, J., and Barrett, S. R.H.: Global budget and radiative forcing of black carbon aerosol: constraints from pole-to-pole (HIPPO) observations across the Pacific, J. Geophys. Res., 119, 195–206, 2014

Wang, X., Zhang, L., and Moran, M. D.: Uncertainty assessment of current size-resolved parameterizations for below-cloud particle scavenging by rain, Atmos. Chem. Phys., 10, 5685–5705,https://doi.org/10.5194/acp-10-5685-2010, 2010.

Wang, X., Zhang, L., and Moran, M. D.: Development of a new semi-empirical parameterization for below-cloud scavenging of size-resolved aerosol particles by both rain and snow, Geosci. Model Dev., 7, 799–819, https://doi.org/10.5194/gmd-7-799-2014, 2014.

Wesely, M. L.: Parameterization of surface resistances to gaseous dry deposition in regional-scale numerical models, Atmos. Environ., 23, 1293–1304, 1989.

Wesely, M. L., Sisterson, D. L., and Jastrow, J. D.: Observations of the chemical properties of dew on vegetation that affect the dry deposition of SO_2, J. Geophy. Res., 95, 7501–7514, 1990.

Wofsy, S.C., S. Afshar, H.M. Allen, E.C. Apel, E.C. Asher, B. Barletta, J. Bent, H. Bian, B.C. Biggs, D.R. Blake, N. Blake, I. Bourgeois, C.A. Brock, W.H. Brune, J.W. Budney, T.P. Bui, A. Butler, P. Campuzano-Jost, C.S. Chang, M. Chin, R. Commane, G. Correa, J.D. Crounse, P. D. Cullis, B.C. Daube, D.A. Day, J.M. Dean-Day, J.E. Dibb, J.P. DiGangi, G.S. Diskin, M. Dollner, J.W. Elkins, F. Erdesz, A.M. Fiore, C.M. Flynn, K.D. Froyd, D.W. Gesler, S.R. Hall, T.F. Hanisco, R.A. Hannun, A.J. Hills, E.J. Hintsa, A. Hoffman, R.S. Hornbrook, L.G. Huey, S. Hughes, J.L. Jimenez, B.J. Johnson, J.M. Katich, R.F. Keeling, M.J. Kim, A. Kupc, L.R. Lait, J.-F. Lamarque, J. Liu, K. McKain, R.J. Mclaughlin, S. Meinardi, D.O. Miller, S.A. Montzka, F.L. Moore, E.J. Morgan, D.M. Murphy, L.T. Murray, B.A. Nault, J.A. Neuman, P.A. Newman, J.M. Nicely, X. Pan, W. Paplawsky, J. Peischl, M.J. Prather, D.J. Price, E. Ray, J.M. Reeves, M. Richardson, A.W.

Rollins, K.H. Rosenlof, T.B. Ryerson, E. Scheuer, G.P. Schill, J.C. Schroder, J.P. Schwarz, J.M. St.Clair, S.D. Steenrod, B.B. Stephens, S.A. Strode, C. Sweeney, D. Tanner, A.P. Teng, A.B. Thames, C.R. Thompson, K. Ullmann, P.R. Veres, N. Vieznor, N.L. Wagner, A. Watt, R. Weber, B. Weinzierl, P.O. Wennberg, C.J. Williamson, J.C. Wilson, G.M. Wolfe, C.T. Woods, and L.H. Zeng, ATom: Merged Atmospheric Chemistry, Trace Gases, and Aerosols. ORNL DAAC, Oak Ridge, Tennessee, USA. https://doi.org/10.3334/ORNLDAAC/1581, 2018.

Xu, J.-W., Martin, R. V., Morrow, A., Sharma, S., Huang, L., Leaitch, W. R., Burkart, J., Schulz, H., Zanatta, M., Willis, M. D., Henze, D. K., Lee, C. J., Herber, A. B., and Abbatt, J. P. D.: Source attribution of Arctic black carbon constrained by aircraft and surface measurements, Atmos. Chem. Phys., 17, 11971–11989, https://doi.org/10.5194/acp-17-11971-2017, 2017.

Yu, F. and Luo, G.: Simulation of particle size distribution with a global aerosol model: contribution of nucleation to aerosol and CCN number concentrations, Atmos. Chem. Phys., 9, 7691–7710,doi:10.5194/acp-9-7691-2009, 2009.

Yu, F., Luo, G., and Ma, X.: Regional and global modeling of aerosol optical properties with a size, composition, and mixing state resolved particle microphysics model, Atmos. Chem. Phys., 12, 5719–5736, https://doi.org/10.5194/acp-12-5719-2012, 2012.

Zender, C. S., Bian, H., and Newman, D., Mineral Dust Entrainment and Deposition (DEAD) model: Description and 1990s dust climatology, J. Geophys. Res., 108, 4416, doi:10.1029/2002JD002775, D14, 2003.

1   Table 1. List of Λ and b values in equation 15 for rain and snow washout parameterizations.

	Rain		Snow	
	T>268 K		248 K<T<268 K	
	Λ	b	Λ	b
GC12				
HNO_3	2.8×10^{-5}	1.0	0	0
Coarse aerosol	2.6×10^{-4}	0.79	4.2×10^{-4}	0.96
Fine aerosol	4.3×10^{-6}	0.61	8.8×10^{-6}	0.96
This work				
HNO_3	3×10^{-3} [‡]	0.62 [‡]	3×10^{-3} [‡]	0.62 [‡]
Coarse aerosol	2×10^{-4} [†]	0.85 [†]	2×10^{-3} [†]	0.7 [†]
Hydrophobic fine aerosol	5×10^{-7} [†]	0.7 [†]	1×10^{-5} [†]	0.66 [†]
Hydrophilic fine aerosol	1×10^{-5} [*]	0.7 [†]	2×10^{-4} [*]	0.66 [†]

2   [†] from Wang et al. (2014) assuming fine aerosol with diameter of 100 nm and coarse aerosol

3   with diameter of 6 μm; [‡] from Luo et al. (2019); [*] this work.

4

5

1 Table 2. Number of sites with surface concentration observation (NVO) and number of sites

2 satisfying criterion (NSC) at surface monitoring networks in the US, Europe, and Asia.

	USA		Europe		Asia	
	NVO	NSC	NVO	NSC	NVO	NSC
SO2	USEPA		EMEP		EANET	
	464	288	42	20	14	3
HNO3	CASTNET		EMEP		EANET	
	84	77	25	8	25	5
NH3	AMoN		EMEP		EANET	
	53	17	40	15	25	10
SO4	IMPROVE+CSN		EMEP		EANET	
	371	214	52	21	25	9
NIT	IMPROVE+CSN		EMEP		EANET	
	371	213	66	22	25	8
NH4	IMPROVE+CSN		EMEP		EANET	
	371	178	66	24	25	9
BC	IMPROVE		EMEP			
	168	122	11	5		
OC	IMPROVE		EMEP			
	168	118	11	5		

3

4

Table 3. Observed and simulated annual mean surface concentrations of aerosols and aerosol precursors in the US, Europe, and Asia. Comparisons include annual mean surface concentrations (M, μg m^{-3}), normalized mean bias (NMB, %), and correlation coefficient (*r*, when # of samples > 10) between observed and simulated annual mean values for the 8 species by G12, L2019, and WETrev cases.

		USA				Europe				Asia		
		G12	L2019	WETrev		G12	L2019	WETrev		G12	L2019	WETrev
SO2	M: 5.61	4.48	4.29	4.32	M: 1.36	2.36	2.16	2.05	M: 2.51	4.08	3.58	3.08
	NMB	-20	-23	-23	NMB	74	59	51	NMB	63	43	23
	r	0.49	0.49	0.48	*r*	0.53	0.50	0.50	*r*			
HNO3	M: 0.83	1.47	0.83	0.83	M: 0.67	1.40	0.66	0.67	M: 0.86	1.90	0.64	0.68
	NMB	78	0.9	0.9	NMB	107	-2.4	-0.7	NMB	121	-26	-21
	r	0.57	0.59	0.60	*r*				*r*			
NH3	M: 1.00	1.02	1.04	1.21	M: 0.83	0.84	0.91	1.07	M: 0.96	0.95	0.88	1.06
	NMB	2.6	4.4	21	NMB	0.9	8.7	28	NMB	-1.7	-8.6	10
	r	0.26	0.28	0.29	*r*	0.90	0.89	0.91	*r*			
SO4	M: 1.30	1.29	0.91	1.17	M: 1.29	1.38	0.87	1.24	M: 2.63	2.77	1.69	2.46
	NMB	-1.1	-30	-10	NMB	6.9	-33	-4.3	NMB	5.5	-36	-6.3
	r	0.92	0.92	0.92	*r*	0.92	0.90	0.92	*r*			
NIT	M: 0.71	1.60	0.78	0.81	M: 1.66	3.77	1.54	1.73	M: 0.60	2.23	0.89	0.83
	NMB	126	10	15	NMB	127	-7.5	4.2	NMB	269	47	37
	r	0.53	0.58	0.61	*r*	0.85	0.86	0.86	*r*			
NH4	M: 0.61	0.89	0.54	0.64	M: 0.88	1.67	0.82	1.02	M: 0.58	1.55	0.82	1.08
	NMB	45	-13	4.1	NMB	90	-7.3	16	NMB	167	42	86
	r	0.76	0.79	0.79	*r*	0.79	0.81	0.81	*r*			
BC	M: 0.20	0.18	0.16	0.17	M: 0.51	0.38	0.32	0.34				
	NMB	-7.0	-20	-14	NMB	-25	-37	-32				
	r	0.54	0.54	0.54	*r*							
OC	M: 1.01	0.80	0.68	0.72	M: 1.97	1.00	0.77	0.85				
	NMB	-20	-33	-29	NMB	-49	-61	-57				
	r	0.63	0.65	0.65	*r*							

Table 4. Relative contribution (%) of modified rainout (RO), washout (WO), rain pH (RP), dry deposition (DD), and aqueous chemistry (AC) to the changes of January and July surface concentrations at the US, Europe, and Asia sites.

	USA					Europe					Asia				
	RO	WO	RP	DD	AC	RO	WO	RP	DD	AC	RO	WO	RP	DD	AC
								January							
SO2	5.0	15.3	0.5	54.2	25.0	11.7	24.1	12.0	19.0	33.1	3.6	15.3	0.2	27.7	53.2
HNO3	15.5	73.4	0.5	5.3	5.2	25.2	60.1	1.3	2.4	11.0	8.7	63.1	0.1	8.4	19.6
NH3	7.9	23.7	1.6	30.5	36.3	9.0	20.4	31.3	14.9	24.4	3.9	7.0	5.8	26.2	57.1
SO4	46.6	17.3	0.4	6.2	29.5	74.3	8.5	0.9	2.1	14.3	29.4	17.5	0.1	5.8	47.3
NIT	37.7	46.7	0.7	5.3	9.6	56.5	34.1	1.4	1.5	6.5	17.4	43.9	0.3	10.7	27.6
NH4	48.7	34.3	0.7	6.0	10.3	78.3	13.2	1.0	2.2	5.2	40.6	22.9	0.3	3.1	33.0
								July							
SO2	5.6	13.1	8.5	50.5	22.3	3.0	31.3	1.3	31.0	33.4	13.3	15.9	15.2	23.5	32.1
HNO3	5.8	91.3	0.5	2.0	0.4	5.2	93.8	0.2	0.7	0.1	11.4	86.8	0.5	1.2	0.1
NH3	6.7	21.7	13.4	49.9	8.2	5.7	53.2	11.5	26.6	3.0	4.8	17.9	28.7	45.0	3.6
SO4	48.7	16.5	4.4	12.9	17.5	66.0	11.7	0.7	3.0	18.7	63.9	16.2	2.6	8.4	8.8
NIT	16.1	68.7	2.7	10.9	1.6	12.3	82.6	1.5	3.2	0.4	24.4	64.7	3.3	6.9	0.7
NH4	35.7	36.4	4.1	13.0	10.8	27.2	63.7	1.0	2.6	5.5	52.6	29.1	3.3	8.9	6.2

Table 5. Number of sites with wet deposition observation (NVO) and number of sites satisfying criterion (NSC) at surface monitoring networks in the US, Europe, and Asia.

	USA		Europe		Asia	
	NTN		EMEP		EANET	
	NVO	NSC	NVO	NSC	NVO	NSC
SO2+SO4	250	86	62	25	53	4
HNO3+NIT	250	86	67	30	53	4
NH3+NH4	250	85	64	29	53	4

Table 6. Observed and simulated annual mean wet depositions of aerosols and aerosol precursors in the US, Europe, and Asia. Comparisons include annual mean wet depositions (M, kg ha^{-1} year^{-1}), normalized mean bias (NMB, %), and correlation coefficient (*r*, when # of samples > 10) between observed and simulated annual mean values by G12, L2019, and WETrev cases. Simulated values at sites were corrected following Paulot et al. (2014) to remove bias due to precipitation.

		USA				Europe				Asia		
		G12	L2019	WETrev		G12	L2019	WETrev		G12	L2019	WETrev
SO2+SO4	M: 10.3	6.8	8.0	9.4	M: 6.3	3.4	5.0	5.9	M: 28.6	10.3	11.1	13.2
	NMB	-35	-23	-9.0	NMB	-46	-21	-6.2	NMB	-64	-61	-54
	r	0.81	0.79	0.81	*r*	0.56	0.55	0.49	*r*			
HNO3+NIT	M: 9.5	9.6	18.1	19.1	M: 9.9	6.8	14.3	14.0	M: 14.6	13.3	15.8	15.5
	NMB	0.6	89	100	NMB	-31	45	42	NMB	-9.2	8.1	6.2
	r	0.9	0.85	0.88	*r*	0.84	0.59	0.64	*r*			
NH3+NH4	M: 3.6	3.2	4.0	4.2	M: 3.9	2.6	3.9	3.6	M: 3.9	3.5	3.3	3.8
	NMB	-10	12	16	NMB	-33	-1.6	-7.7	NMB	-10	-14	-2.5
	r	0.85	0.87	0.85	*r*	0.75	0.55	0.67	*r*			
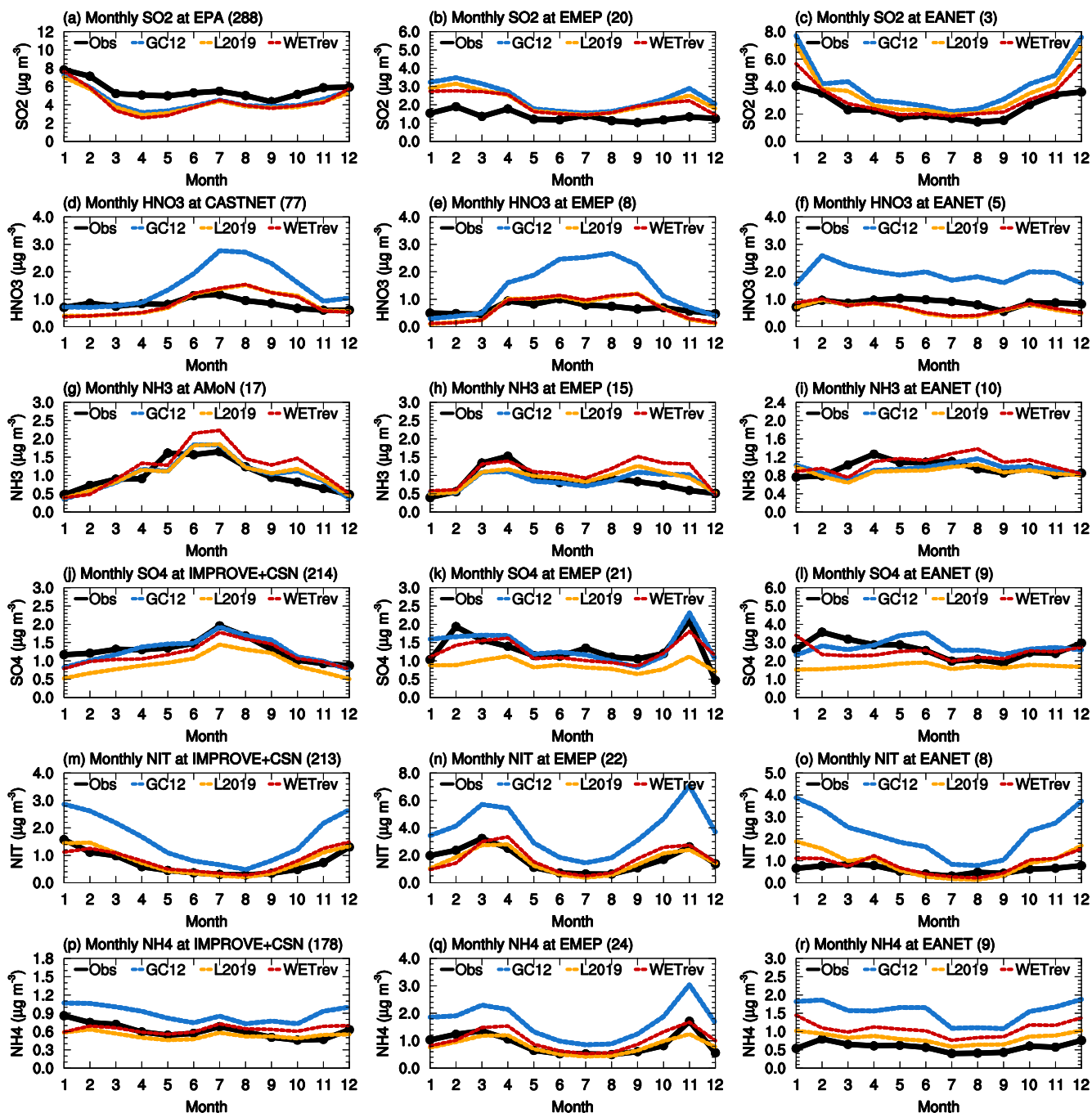
Figure 1. Variations of monthly means for year 2011 showing the comparisons of SO_2, nitric acid, ammonia, sulfate, nitrate, and ammonium surface mass concentrations which are observed over (left column) the US, (center column) Europe, and (right column) Asia sites (black) and simulated by GC12 (blue), L2019 (yellow), and WETrev (red) cases.
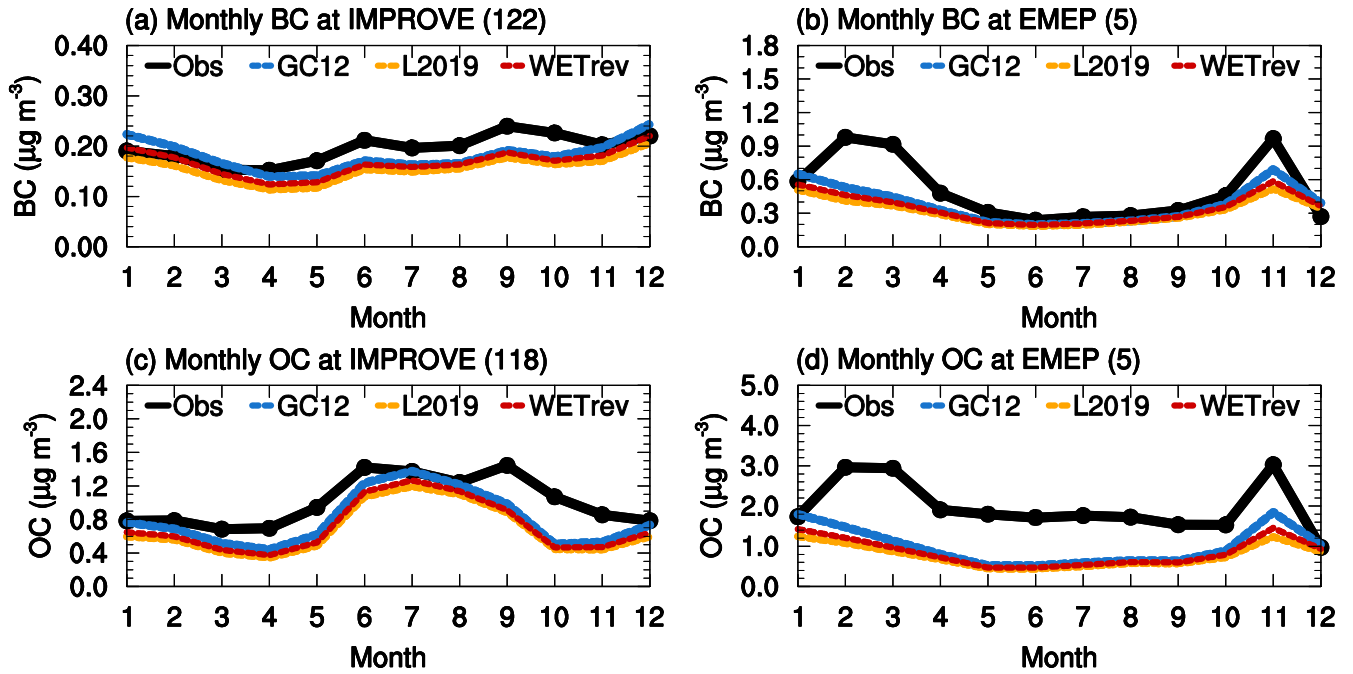
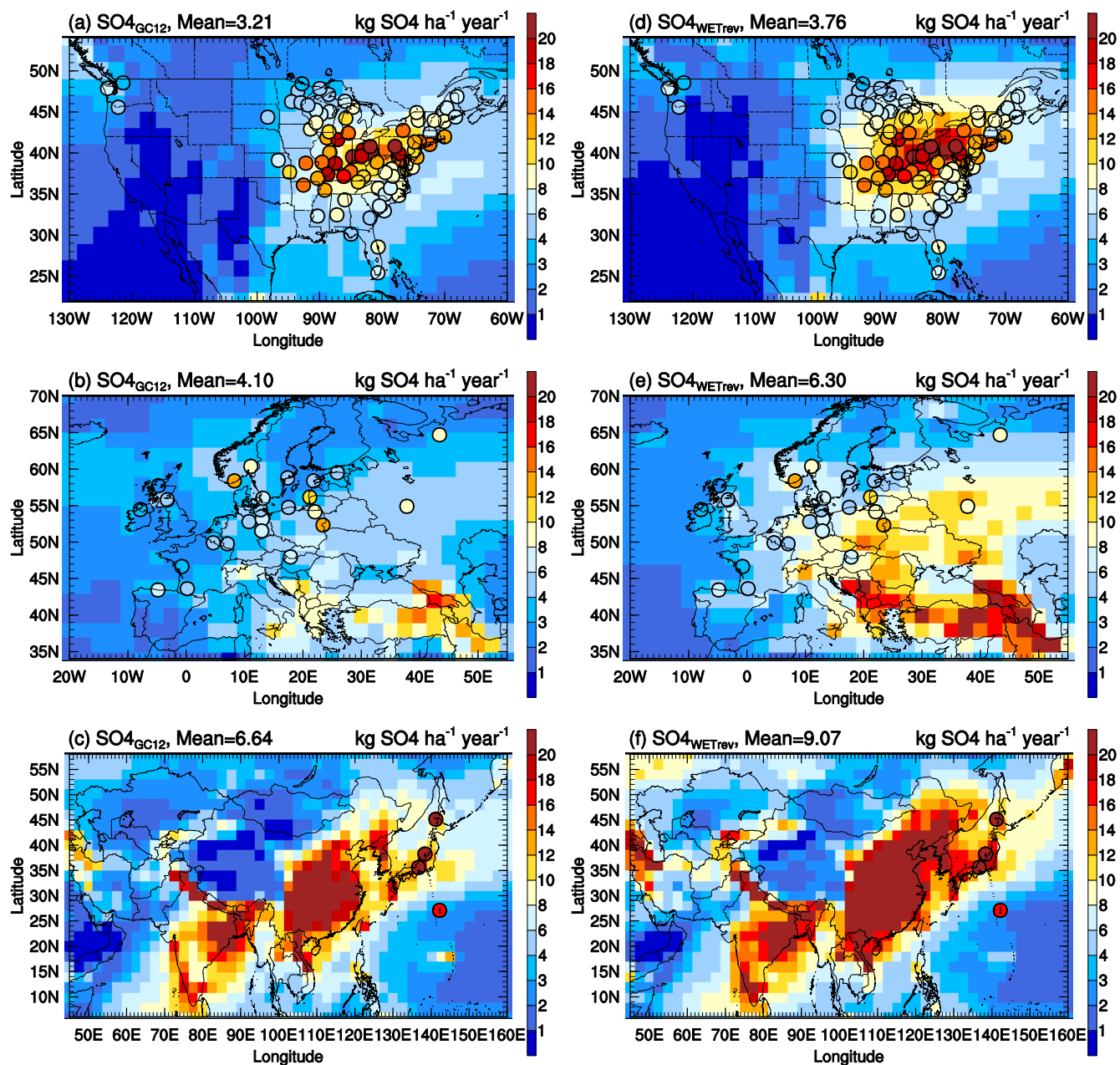Figure 2. Variations of monthly means for year 2011 showing the comparisons of black carbon and organic carbon surface mass concentrations which are observed over (left column) the US and (right column) Europe sites (black) and simulated by GC12 (blue), L2019 (yellow), and WETrev (red) cases.

Figure 3. Horizontal distributions of SO_2+SO_4 deposition over the US (top), Europe (middle), and Asia (bottom). Filled circles are annual mean wet depositions at NTN, EMEP, and EANET corrected following Paulot et al. (2014) to remove bias due to precipitation.
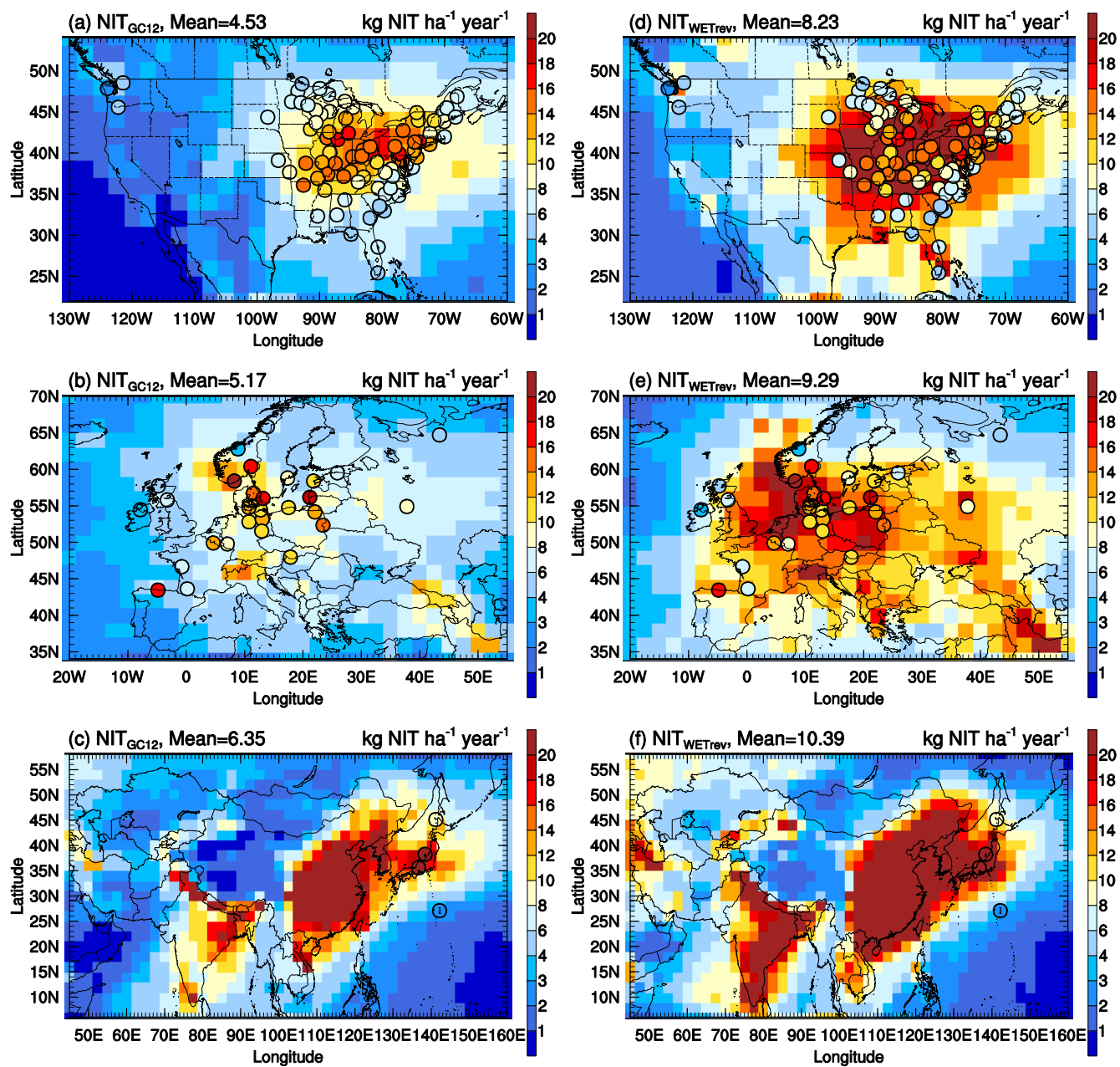
Figure 4. The same as Fig. 3 but for HNO₃+NIT.
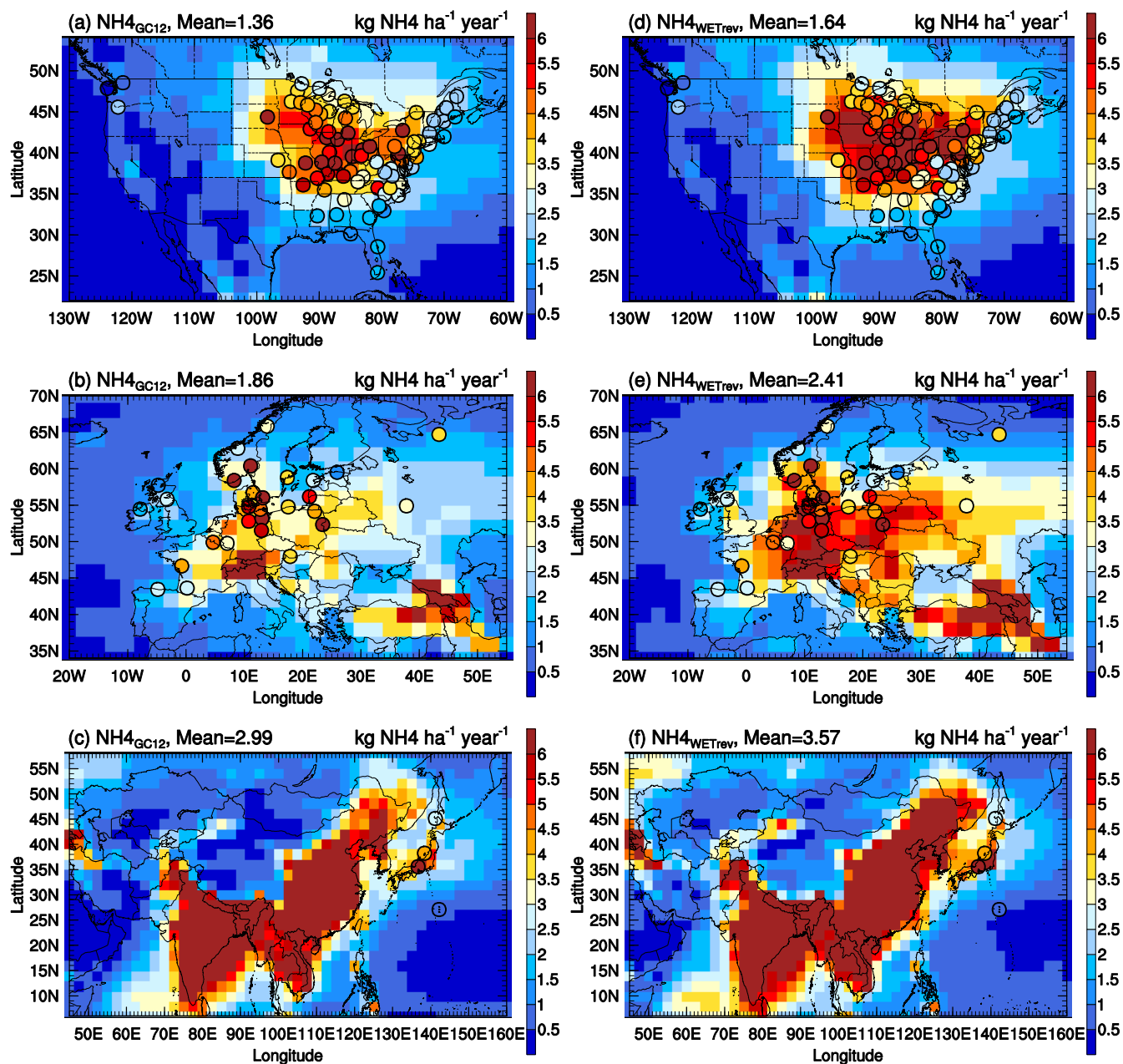
Figure 5. The same as Fig. 3 but for NH₃+NH4.
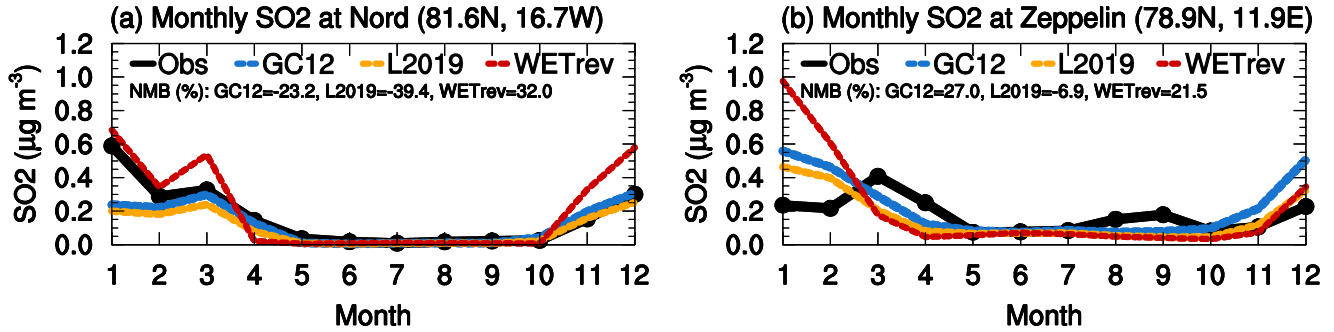
Figure 6. Variations of multiyear monthly means showing the comparisons of SO₂ surface mass concentrations which were observed at (a) Nord (2008-2013) and (b) Zeppelin (2008-2013) sites (black) and simulated (2011) by GC12 (blue), L2019 (yellow), and WETrev (red) cases.
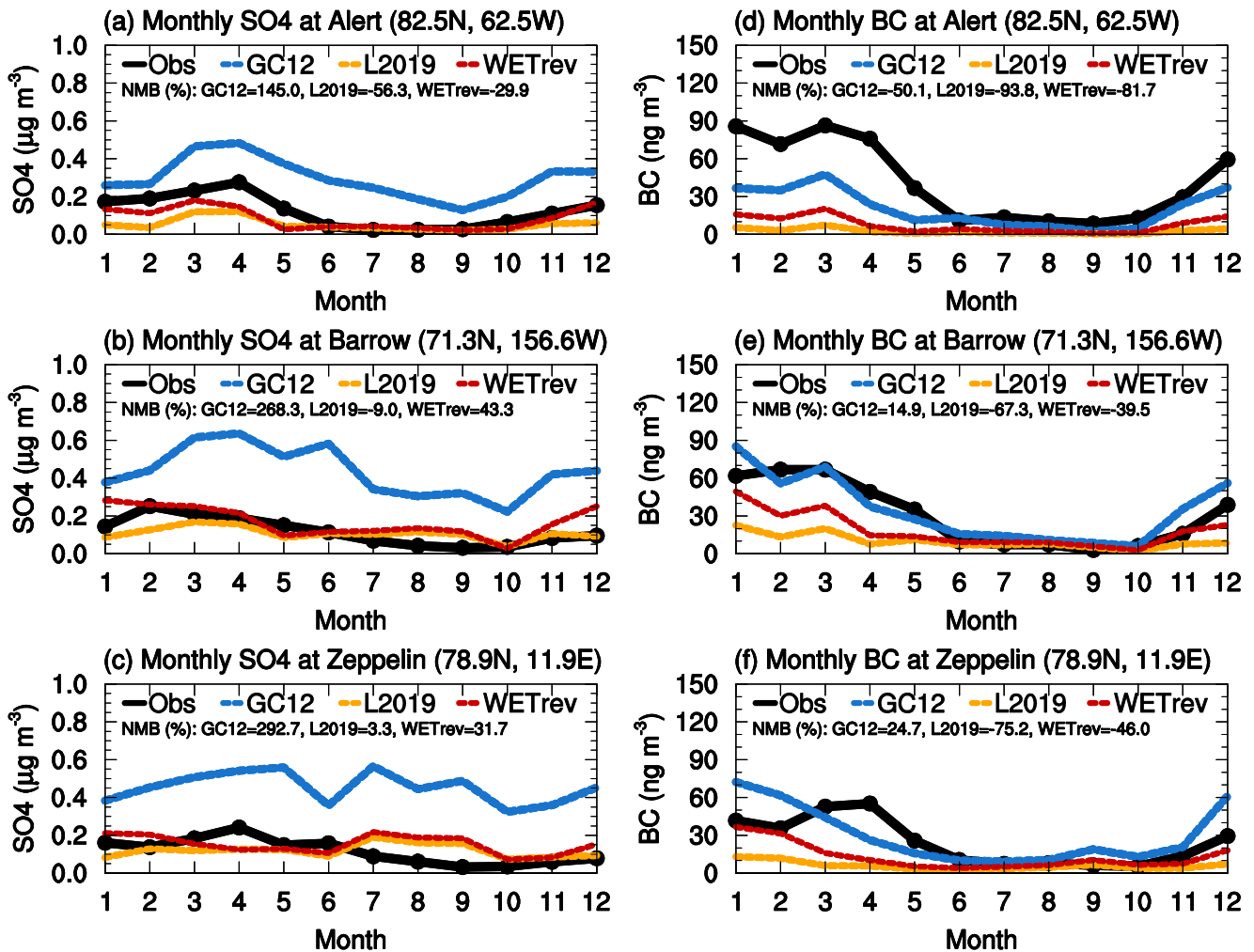
Figure 7. Variations of multiyear monthly means showing the comparisons of (a-c) sulfate and (d-f) black carbon surface mass concentrations which were observed at (top) Alert (2008-2012), (middle) Barrow (2008-2013), and (bottom) Zeppelin (2008-2013) sites (black) and simulated (2011) by GC12 (blue), L2019 (yellow), and WETrev (red) cases.

44
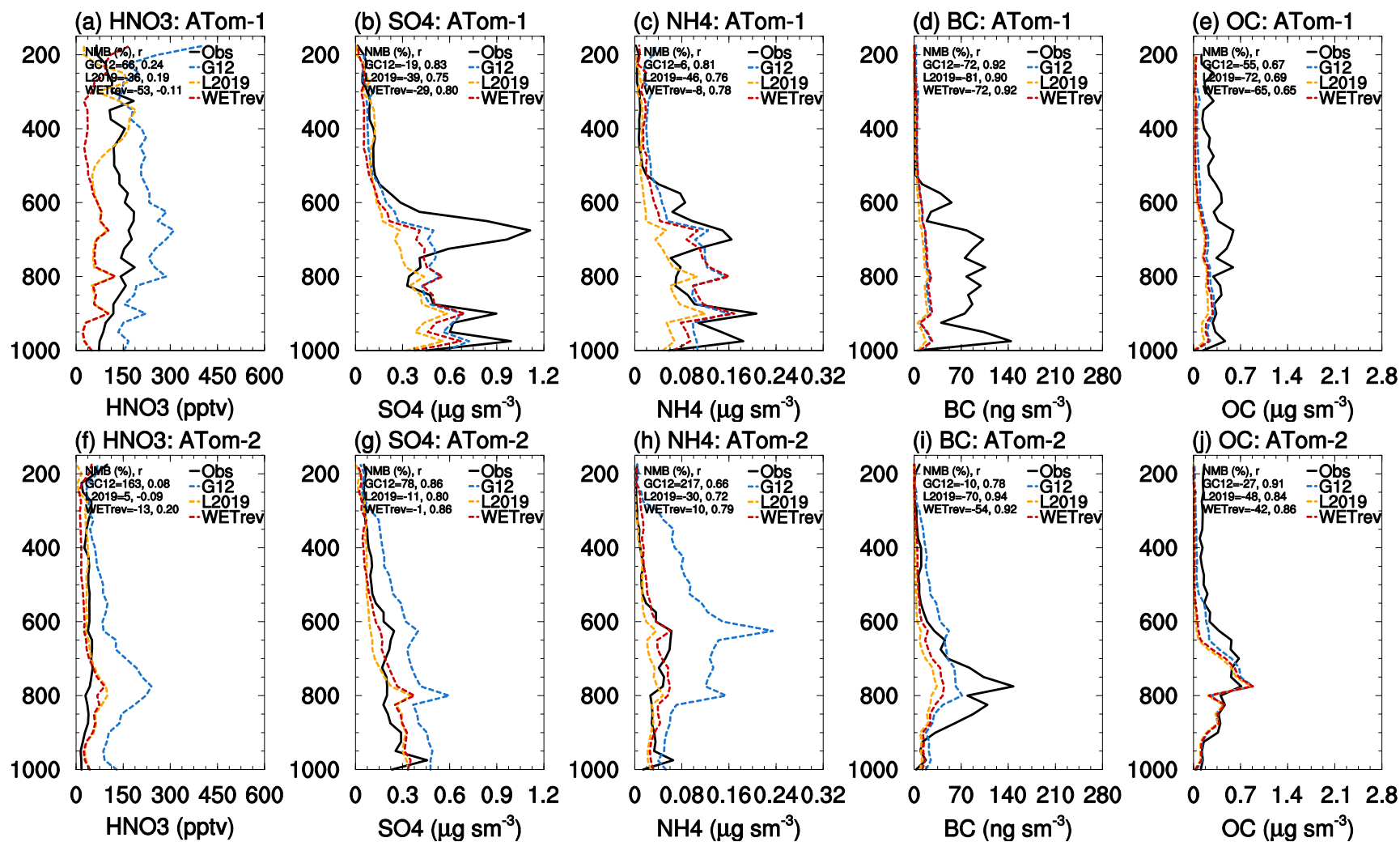
Figure 8. Vertical profiles of nitric acid, sulfate, ammonium, black carbon, and organic carbon from ATom aircraft observations (black, ATom-1: a-e; ATom-2: f-j) and GEOS-Chem simulations by GC12 (blue), L2019 (yellow) and WETrev (red) cases over the Northern hemisphere.
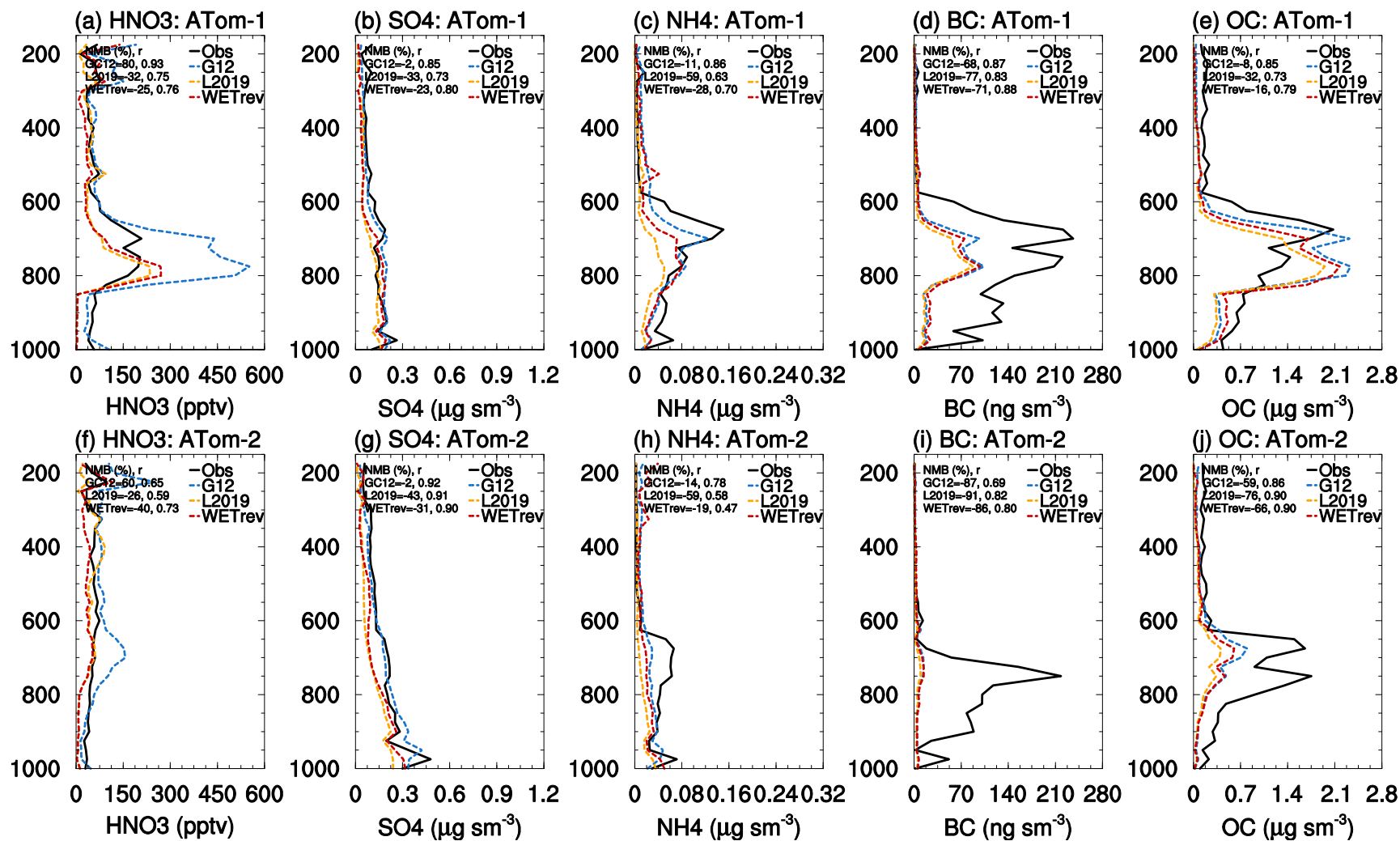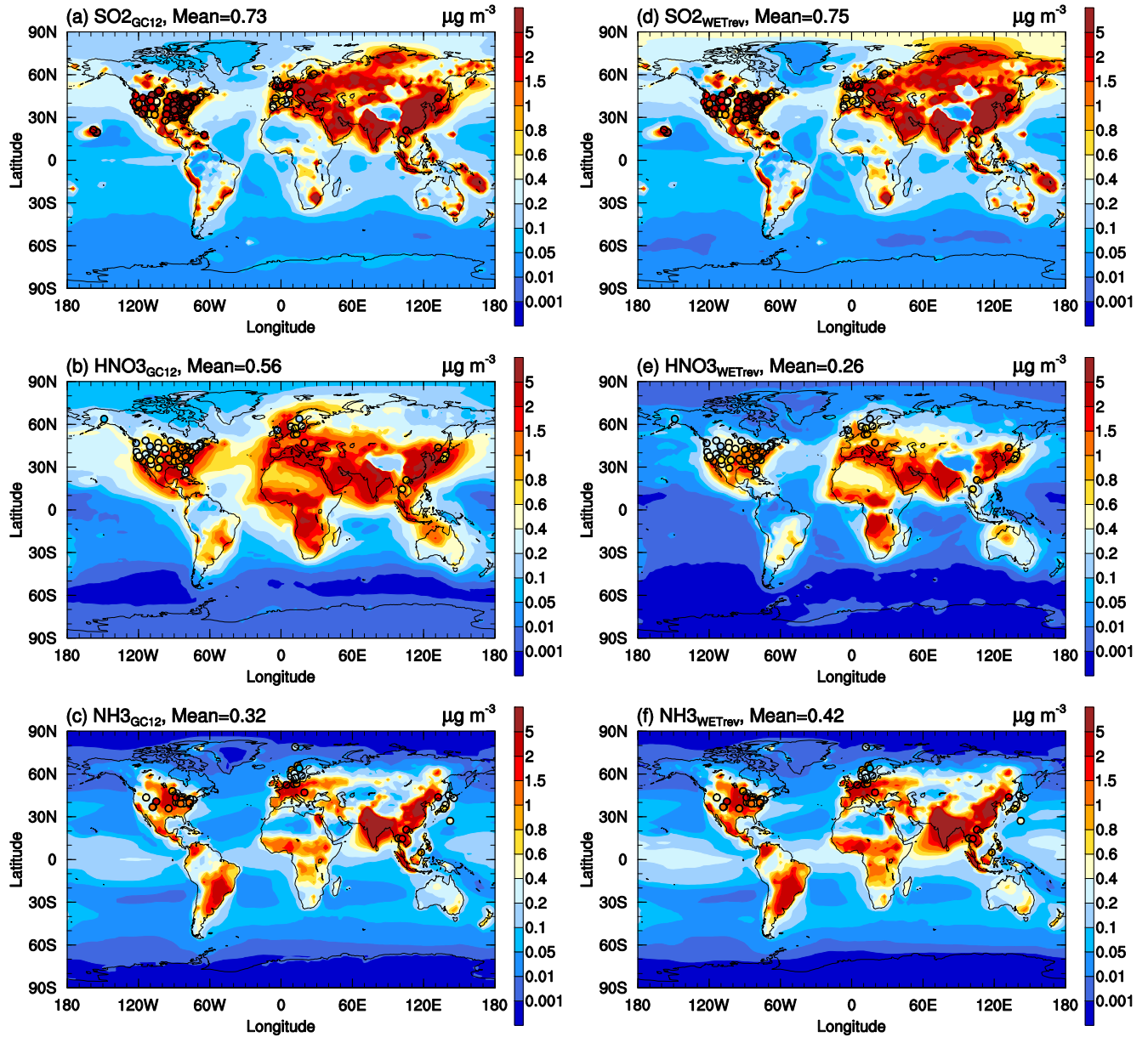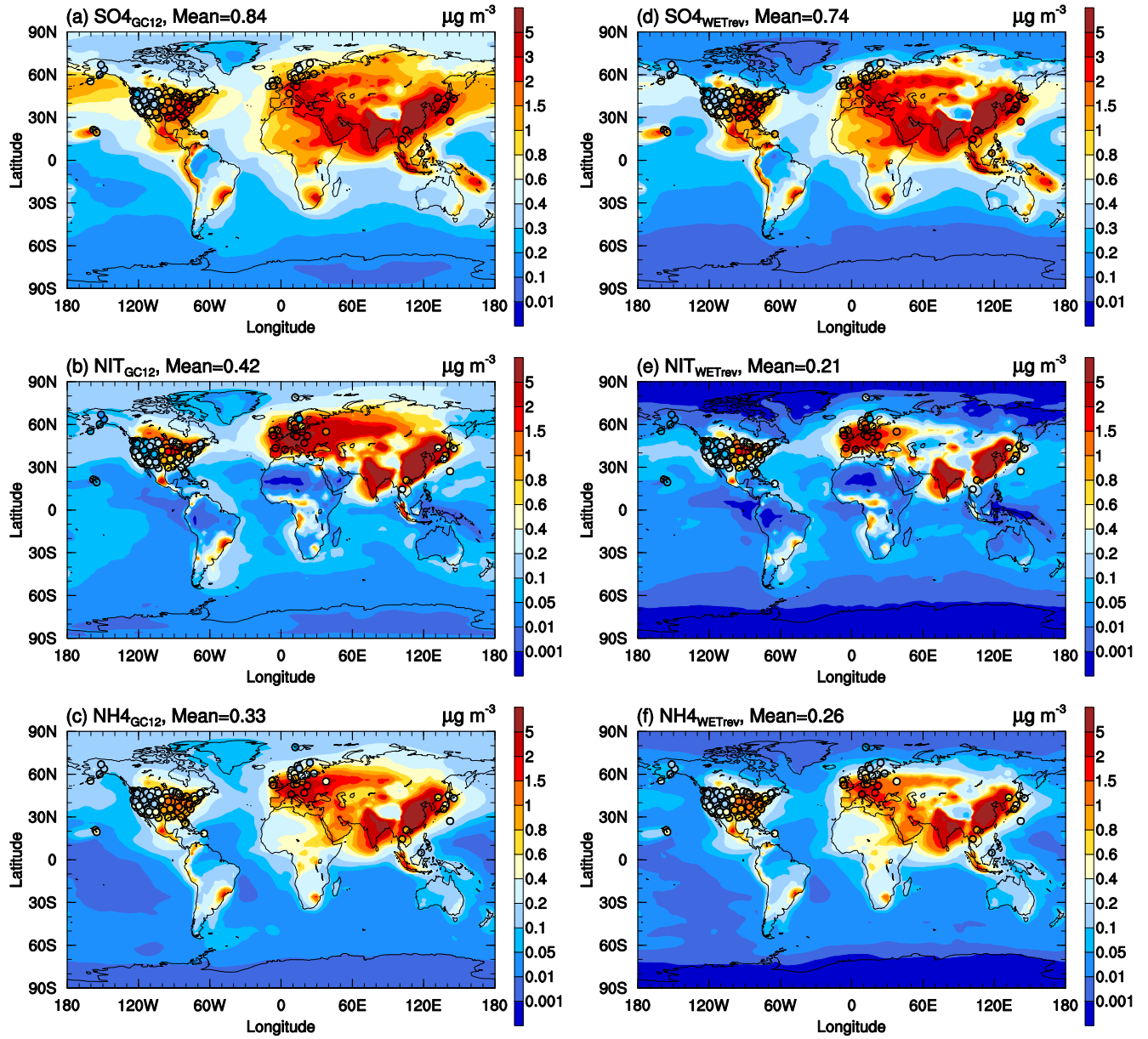
Figure 9. The same as Fig. 8 but over the Southern Hemisphere.

Figure 10. Horizontal distributions of SO$_2$, nitric acid, and ammonia surface mass concentrations simulated by (a-c) GC12 case and (d-f) WETrev case. Filled circles are annual mean surface mass concentrations observed at IMPROVE, CSN, CASTNET, AMoN, EMEP, and EANET for corresponding species.
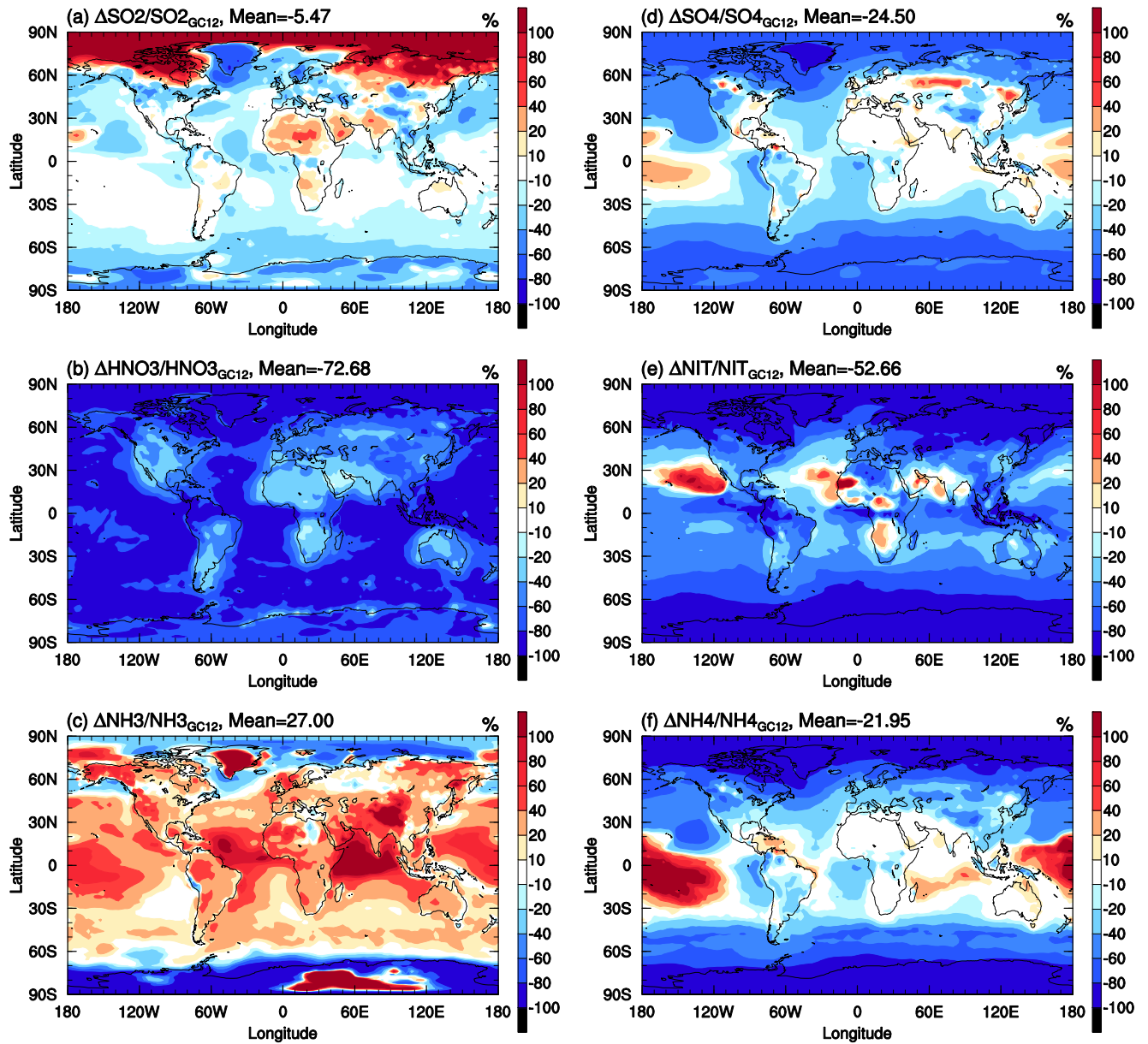
Figure 11. The same as Fig. 10 but for sulfate, nitrate, and ammonium surface mass concentrations.
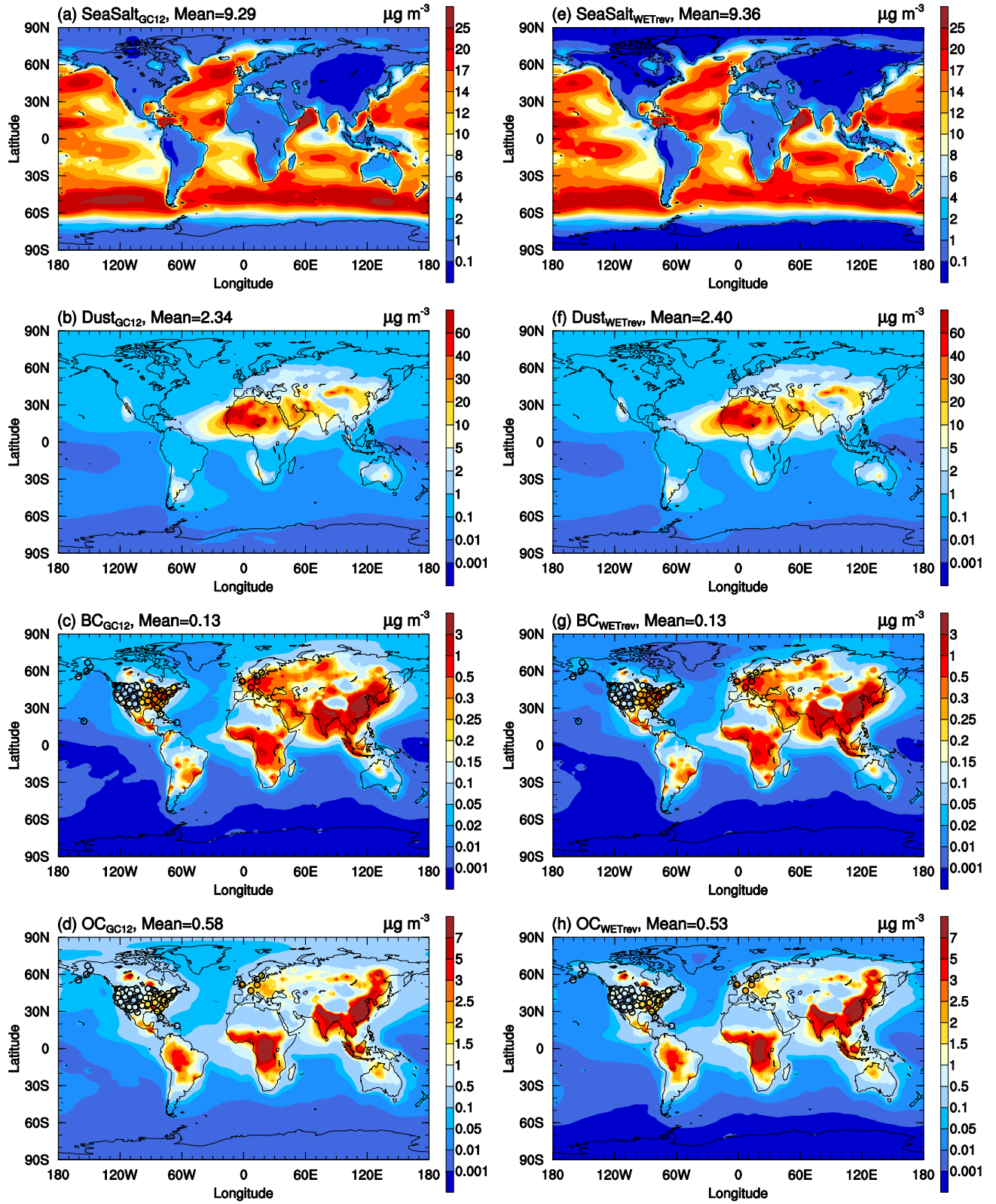
Figure 12. The same as Fig. 10 but for black carbon, organic carbon, sea salt, and dust surface mass concentrations.

Figure 13. Horizontal distributions of percentage changes in annual mean (a) SO$_2$, (b) nitric acid, (c) ammonia, (d) sulfate, (e) nitrate, and (f) ammonium surface mass concentrations due to the switching of GC12 case to WETrev case.
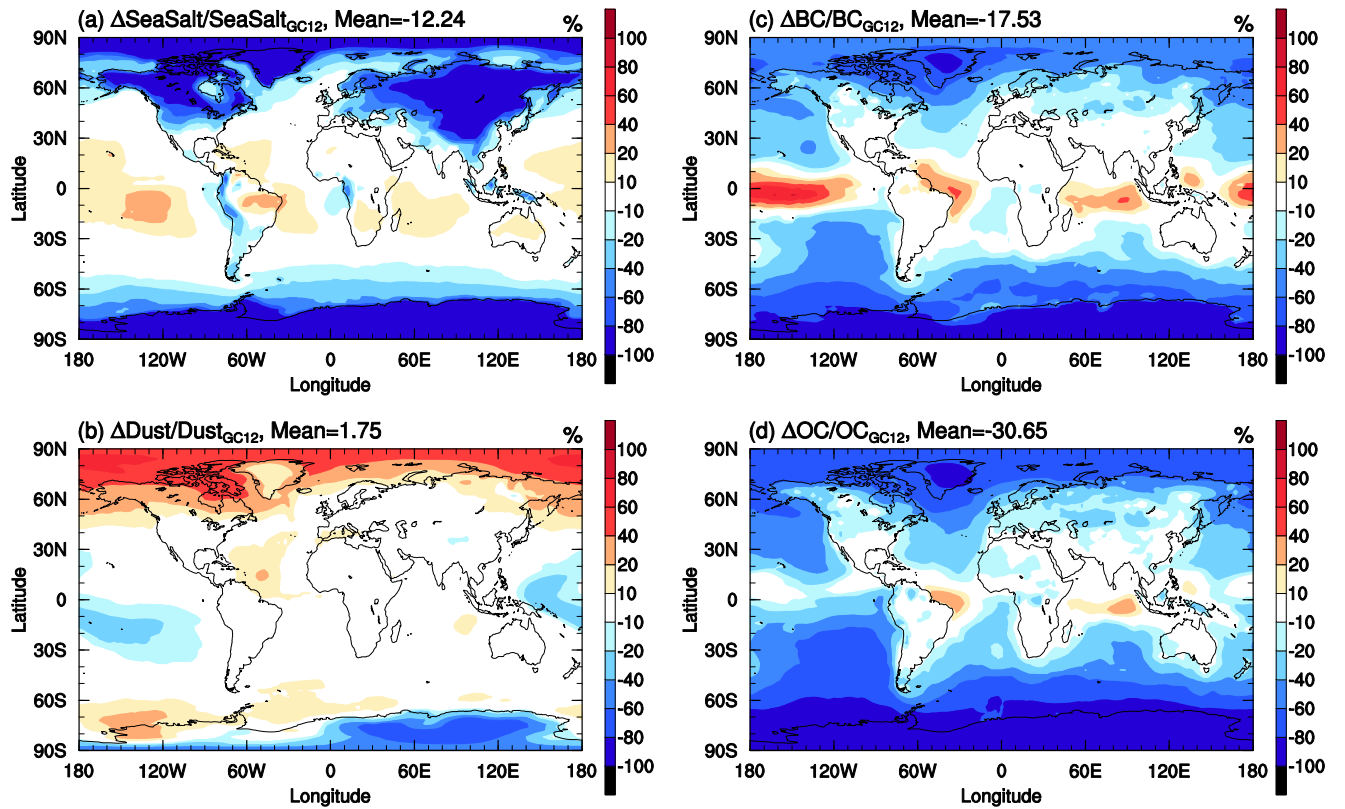
Figure 14. The same as Fig. 13 but for (a) sea salt, (b) dust, (c) black carbon, and (d) organic carbon surface mass concentrations.